Fourier Transform Infrared Spectroscopy as a method of investigation of semiconductor plasma etching

A thesis for the degree of

Master of Science

Submitted to

Dublin City University

By

Chiara Galassi

Research Supervisor

Dr. Enda McGlynn

School of Physical Sciences

Dublin City University

September 2005

Declaration

I hereby certify that this material, which I now submit for assessment on the programme of study leading to the award of Master of Science is entirely my own work and has not been taken from the work of others save and to the extent that such work has been cited and acknowledged within the text of my work.

Signed: Chiara Galassi

Chiara Galassi

Id No.: 54147140

Date: 12/09/2005

List of Figures

List of Tables

Acknowledgments

I would like to thank my supervisor, Dr. Enda McGlynn, for his constant encouragement, professional help, patience, precious advice and friendship.

Many thanks to Dr.Bert Ellingboe, Dr. Greg Hughes, Dr.Vesselin Krastev, for their expert insight and for the accurate and essential evaluation of the experiments carried out.

Thanks to Ian Reid for the constructive discussions about the samples, the intuition in the analysis, and for carrying out essential experiments with XPS, SIMS, and the ellipsometer; thanks to Andrey Isliakin for the helpful hints about the plasma theory.

Thanks to Justina, for her joyful friendship, for the happy atmosphere in the office, and the nice chats on the grass; to Ricky, for the funny jokes, the good laughs, and continuously lifting spirits; to Jean Rene, for his tactful friendship, the smiles, and all the lovely trips around Ireland.

Thanks to Lucia and Domenico, for the relaxing and happy atmosphere they brought inside the house in the last few months, for putting up with me even at my worst moments, and encouraging me every day.

I would like to thanks my parents, for their constant caring and support and for believing in me.

Thanks to Matteo, Francesca, Renzo, for their outstanding affection and patience, for their listening and giving a happier perspective on things.

Thanks to Ahmed, whose simple spontaneity and affectionate care encouraged me to accomplish this study and left inside of me the gift of a deeper awareness for looking at people and life.

Abstract

Plasma etching is a complicated process in the way it involves many ion and neutral species that, depending on plasma conditions, give rise to difficulties in controlling the etch mechanism both from a sputtering and a deposition perspective.

To investigate and understand the dynamics of interactions at the interface between the plasma and the solid, surface characterization techniques are necessary: here we investigate the suitability of FTIR (Fourier Transform Infrared Spectroscopy) as a non-destructive, real-time, characterization method complementary to the standard characterization techniques such as XPS (X-Ray Photoelectron Spectroscopy) and SIMS (Secondary Ion Mass Spectroscopy).

The work presented here therefore focuses the attention on both etched silicon dioxide substrates and ultra low dielectric substrates, with the purpose of studying and characterizing the surface modification due to reactions with the etching components and products, in particular to the presence of chemical bonds between silicon and fluorine and carbon.

The possibility of non-destructive infrared detection of the sample surface condition would be of great help as it could be suitable for in-line characterization of the semiconductor devices during manufacturing.

CHAPTER 1: INTRODUCTION

As advanced integrated circuits have evolved to sub-micron generations (dimensions less than 0.1μm) and the integration scale continues to shrink, the interconnect density must be enhanced by decreasing the metal pitch and increasing the number of interconnect metal layers. Along with this both interconnect wiring resistance and capacitance increase, leading to higher interconnect resistance · capacitance (RC) delay time.

Efforts to reduce RC delay and the parasitic capacitance of multilevel interconnections (such as by reducing resistances of metal lines and/or reducing capacitance among metal lines) have been made. Approaches include trying to replace traditional metallization material with lower resistivity materials (aluminium with copper) and using low-k ($k<3.0$) or ultra low-k ($k<2.4$) dielectrics as the intermetallic dielectric materials or interlayer dielectrics (IMD, ILD). All these approaches have the ultimate goal of increasing the device speed [1].

In recent years many studies of organic and inorganic films and polymers that might replace the conventional silicon dioxide (SiO_2, material which is also used as gate oxide in transistors) as interlayer dielectrics have been reported. Among them, due to the low values of their dielectric constants, compounds such as fluorine-doped SiO_2, carbon-doped SiO_2 (SiOCH), metal silsesquioxane (MSQ) and hydrogen silsesquioxane (HSQ) (usually referred to low-k polymers) are considered as the most promising low-k materials. In compounds with $Si\text{-}CH_3$ bonding the lower polarizability of carbon helps to reduce the dielectric constant [2]. But in order to represent a real and useful advantage, these materials should be compatible with the conventional integration processes and not show a significant degradation as a result of these processes.

High-resolution pattern transfer and selective masking layer removal (selective etching of dielectric layers) by plasma etching are two of several key processes required for fabricating silicon-based integrated circuits. Oxygen and fluorocarbon-based plasma treatments of both SiO_2 and low-dielectric constant films are an important processing step

in integrated circuit manufacturing; the plasma conditions (such as pressure, radiofrequency power, treatment time) might have repercussions on the quality of the material, this is why process optimization and understanding of the complexity of the etch mechanism and its effects on the materials is necessary [3]. This is the reason why an accurate analysis of the effects of the etching process is needed, in order to evaluate if the dielectric properties of the film, together with film thickness have been degraded during the process [4, 5].

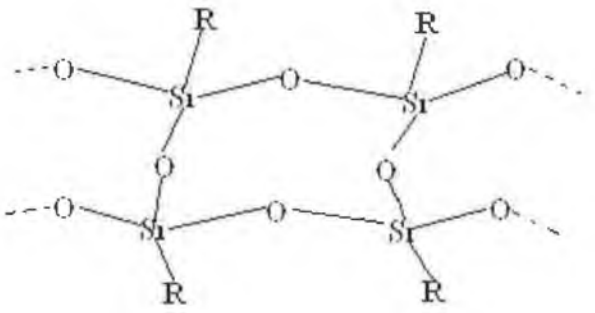

Figure1.1: Generalized schematic example of a polysilsesquioxane structure: in general such structures can be represented in terms of a silsesquioxane-based ULK structure in which each silicon atom is bound to an average of one and a half oxygen and to one hydrocarbon group (represented by R) [6]

Additionally, fluorocarbon films prepared by plasma enhanced chemical vapour deposition (CVD) have attracted increasing interest as one of the most promising materials for interlayer dielectrics because of its low dielectric constant. In order to achieve the goals of the process, it is also highly necessary to understand and control the plasma-surface interactions in this environment [7].

To this purpose a variety of techniques such as X-ray Photoelectron Spectroscopy (XPS), Fourier Transform Infrared Spectroscopy (FTIR), Secondary Ion Mass Spectroscopy (SIMS), can be used to analyze the effect of the plasma treatment on the low-k film [8].

In fact, for a full understanding of the properties and reactivity of a surface, several types of information are required: physical topography, chemical composition, chemical

structure, electronic state, detailed description of bonding of molecules at the surface. But no technique can provide all these pieces of information, and several techniques are always required.

In XPS x-ray photons of precisely defined energy bombard the surface and the kinetic energies of the electrons emitted from the orbitals of the component atoms are measured: the electron binding energies determined in this way enable the component surface atomic composition to be determined. The penetration depth of this technique is of the order of the top ten or so layers of the surface.

In SIMS a beam of high energy (~ keV) primary ions bombards the surface so that secondary atomic and cluster ions emitted can be analysed with a mass spectrometer., and their chemical origin determined via mass measurement.

In both techniques the surface sensitivity depends on the depth of origin of the detected species. Thus in XPS whilst the x-ray photons which bombard the surface can penetrate deep into the solid, the resultant emitted electrons which can be detected without loss of energy can only arise from within 1-4 or 8 nm of the surface. Electrons generated deeper in the solid may escape, but on the way they will have collided with other atoms and lost energy. They are no use for analysis. Similarly in SIMS the surface is bombarded by high energy ions. They deposit their energy down to 30 or 40 nm. However, 95% of the secondary ions which are sputtered out of the solid arise from the top two layers (around 0.6nm) [9]. Depth information can be obtained in SIMS however as the sample is progressively sputtered away and thus interior layers are being constantly exposed over time.

The above mentioned techniques, however, require UHV and can not be used in higher pressure plasma environments. Even if UHV surface analysis provides good information on surface chemistry, it's still unclear how such information can be used under plasma environments to develop new processes and optimize existing ones. For this purpose, real-time monitoring techniques of surfaces for developing and optimizing plasma

processes represent a considerable utility. FTIR and ATR (attenuated total reflection)-FTIR are among the best available techniques to study surfaces in situ and in real time (even during sample processing), since they don't need substantial sample preparation, UHV conditions and are non-destructive. ATR is more sensitive to surface effects and species, due to the evanescent nature of the probing wave [10,11], however the optics required for such measurements are more sophisticated than FTIR in its simplest, single beam, form. A number of workers have successfully used ATR to study surface localised species during, or off-line to, plasma processing [12, 13]. The simplicity of the basic FTIR configuration has led us to examine its potential for the study of the effects of plasma processing on dielectric layers. Because of the large number of high energy species and reactions in an industrial processing chamber, one might expect that the effects of the processing may extend well beyond the few monolayer level, for which ATR is most suitable. These species and reactions may generate observable effects over a large depth in the thin films, observable by conventional FTIR.

FTIR is a potentially good method for analyzing the bonding state of the dielectric layers: as a vibrational spectroscopy technique it helps to elucidate molecular bonding and molecular structure due to the absorption of polychromatic radiation of specific energies corresponding to molecular group vibrations. Quantitative information about the molecular bonding chemistry and chemical functional groups can thus be obtained [5].

Thus the aim of this work is to study the capability of Fourier Transform Infrared Spectroscopy (FTIR) to investigate the properties of both SiO_2 and ULK (Ultra Low-k) etched films and it's potential to elucidate the effects of the plasma interaction in the etching process on these properties. In particular for the case of dielectrics and ULK dielectrics especially, the introduction of species such as carbon and fluorine into the dielectric film during etching (dielectric poisoning) may change the dielectric constant in an uncontrolled manner leading to less efficient device performance and yield [14, 15]. While the concentrations of such contaminants may be measured off-line using equipment such as XPS and SIMS with high sensitivity, these techniques require sophisticated apparatus involving ultra-high vacuum (UHV) chambers as mentioned

earlier. The possibility of an "in-situ" characterization would provide more detailed understanding of the structure-formation dynamics during the plasma processing and would avoid the exposure of the samples to air during transfer [16]. The optical techniques of FTIR and ATR would be more suitable in this regard. The simple configuration of FTIR is particularly attractive and would provide a much simpler on-line (or off-line) characterisation with a minimum amount of sample preparation required. This attractive aspect underlies the goal of this work.

In addition, in our analysis, we also have used ellipsometer in order to get information about the thickness of the sample. Ellipsometry is a very useful technique, being able to perform a sensitive measurement using polarized light to characterize thin films and surfaces [4]. It exploits an incoming light beam of a known polarization state is incident on the sample and the ellipsometer measures the change in the reflected beam's polarization.

This work is made up of two theoretical chapters focusing on optical and electrical properties of semiconductor materials and a general overview on plasma processes, respectively. In chapter two, attention is focused on the optical properties of materials relevant to the spectroscopic techniques used here. The third chapter deals with the chemistry of the plasma and its applications in ultra large scale device integration processes. Chapter four discusses the principles of FTIR, describing the physics behind the technique and the experimental setup. Chapter five describes the samples that have been analyzed and the results of the infrared analysis with reference to, and comparison with, the other experimental techniques, used as a part of the overall project. The last chapter discusses the experimental results and takes into consideration possible future recommendations and methods to optimize the technique based on the previous results.

References

[1] Cheonmam Shim, jaeyoung Yang, Seungman Jung,Donggeun Jung: Thin Solid Films 415 83-87, (2002) .

[2] Sang M.Han and Eray S.Aydil:J.Vac.Sci.Technol. A 15(6), Nov/Dec 1997.

[3] Y.H.Wang, R.Kumar, X.Zhou, J.S.Pan, J.W.Chai: Thin Solid Films 473, 132-136, (2005).

[4] Oehrlein, Doemling, Kastenmeier, Matsuo, Rueger, Schaepkens, Standaert: "Surface science issues in plasma etching", 1998.

[5] "Vibrational spectroscopy of ultra-low dielectric materials", Future Fab. International Issue, volume 17, Metrology Analysis.

[6] Li, Ling, Xuefeng, Fukasawa, Gottlieb, Barela, Anderson: J.Vac.Sci.Technol A 21 (1), Jan/Feb 2003.

[7] Takahashi, Itoh, Nakamura, Tachibana: Thin solid films 374, 303-310, (2000)

[8] K.Maex, M.R.Baklanov, D.Shamiryan, F.Iacopi, S.H. Brongersma, Z.S. Yanovislava, "Low dielectric constant materials for microelectronics", Journal of applied Physics, vol.93, n.11, June 2003.

[9] John C.Vickerman, "Surface analysis-The principal techniques", John Wiley and Sons, 1997.

[10] E.S.Aydil, R.A.Gottscho, Y.J.Chabal, "Real-time monitoring of surface chemistry during plasma processing", Pure and Appl. Chem., Vol.66, No.6, pp.1381-1388, 1994.

[11] P.J.Van den Oever, I.J.Houston, M.C.M. Van de Sanden, W.M.M.Kessels, "Attenuated total reflection infrared spectroscopic study of hydrogenated amorphous and microcrystalline silicon film evolution", Dept. of Applied Physics, Eindhoven University of Technology.

[12] N.Posseme, T.Chevolleau, O.Joubert, L.Vallier, N.Rochat, "Etching of porous SiOCH materials in fluorocarbon-based plasmas", J.Vac.Sci.Technol. B 22(6), Nov/Dec 2004.

[13] Akihito S., Kenta A., Mizuho M., Isao K., Yasushi A., " FTIR-ATR evaluation of Organic Contaminant Methods for SiO_2 Surfaces", Analytical Sciences, Nov.2003, Vol.19.

[14] Y.-H. Kim, M. Hwang, H. J. Kim, J. Y. Kim, Y. Lee, " Infrared spectroscopy study of low-dielectric-constant fluorine-incorporated and carbon-incorporated silicon oxide films", Journal of Applied Physics, Volume 90, N.7, 1 October 2001.

[15] D. Shamiryan, M. R. Baklanov, S. Vanhaelemeersch, and K. Maex, "Comparative study of SiOCH low- k films with varied porosity interacting with etching and cleaning plasma", J. Vac. Sci. Technol. B 20.5., Sep/Oct 2002.

[16] J.Meichsner, K.Li, " In situ characterization of thin-film formation in molecular low-temperature plasmas", Appl-Phys. A 72,565-571 (2001).

CHAPTER 2: ELECTRICAL AND OPTICAL PROPERTIES OF SEMICONDUCTORS

2.1: Electromagnetic waves in semiconductors

When an electromagnetic wave interacts with a semiconductor, the situation is made more complicated than the free space scenario, since, unlike free space, a solid contains both mobile free charges (conduction band electrons and valence band holes) and bound charges (atomic charges and inner electrons tightly localized at the atomic nuclei). The current and the charge density of the free carriers and the polarizability of the bound ones affect Maxwell's equations which need modifications to take account of the charge and current sources [1].

Starting with the contribution of the bound charges, these produce a polarization P, dipole moment per unit volume, that is proportional to the electrical field E and generally lying in the same direction, giving rise to the linear approximation relation

$$P = \chi \cdot \varepsilon_0 \cdot E , \tag{2.1}$$

where the constant χ is the susceptibility and ε_0 the permittivity in the free space ($8.85 \times 10^{-12} C^2 N^{-1} m^{-2}$); consequently the displacement vector* equation is

$$\vec{D} = \varepsilon_0 \vec{E} + \vec{P} = \varepsilon_0 (1 + \chi)\vec{E} = \varepsilon_{lat}(\omega)\varepsilon_0 \vec{E} \tag{2.2}$$

where $\varepsilon_{lat}(\omega)$ is the dielectric response function that describes the polarization, coming from the electrons bound to the lattice atoms themselves, whose polarization depends on the frequency of the electric field.

The current due to free carriers can be related to the electric field by microscopic version of Ohm's law

$$\vec{j} = \sigma(\omega)\vec{E} \tag{2.3}$$

---

* By definition the displacement vector is $\vec{D} = \varepsilon \varepsilon_0 \vec{E}$

where $\sigma(\omega)$ is the conductivity, generally a frequency–dependent quantity. Substituting the equations (2.2) and (2.3) into Maxwell's equations for free space and manipulating to eliminate B, gives the wave equation for the electric field in a solid

$$\nabla \times \nabla \times \vec{E} = \nabla^2 \vec{E} - \nabla(\nabla \cdot \vec{E}) = \varepsilon_{lat}\varepsilon_0\mu_0 \frac{\partial^2 \vec{E}}{\partial t^2} + \sigma\mu_0 \frac{\partial \vec{E}}{\partial t} \tag{2.4}$$

where the term $\nabla \cdot \vec{E}$ indicates the presence of longitudinal waves and the last term on the right includes the current due to free charges. To simplify the analysis it is convenient to assume a plane wave solution $\vec{E} = \vec{E}_0 e^{i(qz-\omega t)}$ to substitute into equation (2.4), resulting in

$$q^2\vec{E} - \vec{q}(\vec{q} \cdot \vec{E}) = \varepsilon_{lat}\varepsilon_0\mu_0\omega^2\vec{E} + \sigma\mu_0 i\omega\vec{E} = \omega^2\varepsilon(\omega)\varepsilon_0\mu_0\vec{E} \tag{2.5}$$

In the last term on the right, the quantity $\varepsilon(\omega)$ represents the total dielectric response function

$$\varepsilon(\omega) = \varepsilon_{lat}(\omega) + \frac{i\sigma(\omega)}{\varepsilon_0\omega} \tag{2.6}$$

This dielectric function resulting from the contribution of both bound charge and free carrier current, is a frequency-dependent quantity and describes the electromagnetic-field / semiconductor interaction in the linear response limit. To solve equation (2.5) it is useful to express E as the sum of transverse and longitudinal components:

$$\vec{E} = E_t\hat{t} + E_q\hat{q} \tag{2.7}$$

where is $\hat{t}$ the unit vector in the x-y plane perpendicular to direction of propagation, and $\hat{q}$ a unit vector along $\vec{q}$.

With this decomposition, equation (2.5) becomes

$$\left[\left(\frac{\omega}{c}\right)^2 \varepsilon(\omega) - q^2\right] E_t\hat{t} + \left(\frac{\omega}{c}\right)^2 \varepsilon(\omega) E_q\hat{q} = 0 \tag{2.8}$$

Since the two terms are linearly independent, the equation is satisfied only if the coefficients of $\hat{t}$ and $\hat{q}$ are each zero. Hence,

$$q^2 = \frac{\omega^2}{c^2}\varepsilon(\omega) \tag{2.9}$$

is the general dispersion relation for transverse waves in a solid of total dielectric function $\varepsilon(\omega)$, and $\varepsilon(\omega)=0$ is the condition for longitudinal waves to exist. For the most part we are interested in the coupling of transverse waves propagating in free space into the semiconductor, and hence will confine our attention to transverse waves in the semiconductor. Bearing in mind that $\varepsilon(\omega)$ is a complex quantity, the magnitude q of the wavevector is also a complex quantity $q = q_R + iq_I$, which, inserted into the plane wave solution of the equation (2.4), results in

$$\vec{E} = \vec{E}_0 e^{-q_I z} e^{i(q_R z - \omega t)} \tag{2.10}$$

In the above equation it is clear that the imaginary part of the wavevector gives a damping of the electric field as it penetrates inside the medium, whereas the real part describes the propagation of the electromagnetic wave inside the medium.

Introducing a more useful notation for optical usage, the complex index of refraction can be introduced

$$\bar{n}(\omega) = n(\omega) + ik(\omega) = \sqrt{\varepsilon(\omega)} \tag{2.11}$$

Then combining equations (2.9),(2.10),(2.11) gives

$$\vec{E} = \vec{E}_0 e^{-kq_0 z} e^{i(nq_0 z - \omega t)} \tag{2.12}$$

where $q_0 = \omega/c$ is the wavevector in vacuum. Equation (2.12) shows that the real part of the refraction index, related to the propagation of the wave trough the definition of propagation velocity $v = \omega/(nq_0)$, is $n = c/v$, nevertheless the imaginary part is related to exponential damping of the wave as it penetrates the medium $e^{-kq_0 z}$.

This latter observation accounts for the name given to k, which is the 'extinction coefficient'.

2.2: Physical quantities for optical characterization of semiconductors

Even though knowing the frequency dependence of the dielectric constant of a solid means knowing the overall optical response, actual measurements are made under macroscopic conditions, where such information may not be readily determined.
In standard spectroscopy, such as carried out in the infrared region, the sample is usually a slab with flat faces and the measured amount of light reflected at the front surface or transmitted trough the back surface depends on the geometry of the sample.
In Raman and photoluminescence spectroscopy the measured quantities are scattered intensity and emission intensity, respectively. In infrared spectroscopy the measured quantity is the sample absorbance as a function of wavelength; but the behaviour of the light at the air-semiconductor interface may still be important to determine the conditions and meaning of the measurement.

For any kind of spectroscopy if the sample is not a single slab of material, but consists of layers of semiconductors, each interface between different materials affects the impinging electromagnetic waves. The fraction of reflected and transmitted light at the interface between two materials can be derived knowing the boundary conditions for Maxwell's partial differential equations.

Consider a typical sample, a slab of thickness d formed of a single type of semiconductor (Figure 2.1).

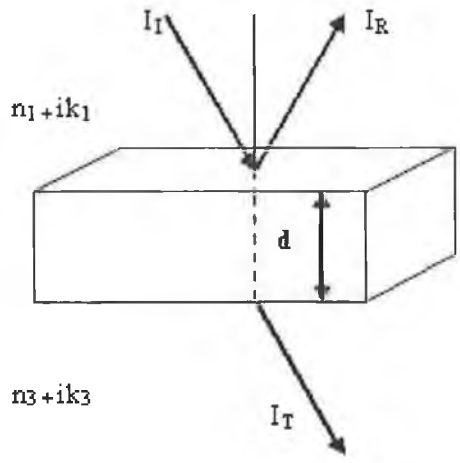

Figure 2.1: A semiconductor sample of thickness d (medium2), between media 1 and 3, showing incident, reflected and transmitted intensities. The reflectance and transmittance are determined by the complex refractive index

Reflectance and transmittance depend on the angle of incidence of the radiation, and the material parameters of regions 1, 2 and 3.

Consider the simple case in which we have normal incidence, and the interface is perpendicular to the direction of propagation, $+z$. In the most familiar case in which media 1 and 2 are air, with $n_1 = 1, k_1 = 0$ and the slab a semiconductor with $\bar{n} = n + ik$, the fractions of incident intensity reflected and transmitted are, respectively :

$$R = \frac{(n-1)^2 + k^2}{(n+1)^2 + k^2} \tag{2.13a}$$

and

$$T = \frac{4}{(1+n^2) + k^2} \tag{2.13b}$$

This gives only the first surface reflectance, but if the sample is semi-infinite along the z axis or the back surface can be considered as infinitely distant this is the complete reflectance. This is the case whenever the sample absorbs light heavily so that little light reaches the back surface. Often over part of the spectral range it is possible to approximate $n > 1$ and $k << 1$ so that

$$R = \frac{(n-1)^2}{(n+1)^2} \tag{2.14}$$

In this case the reflectance behaviour represents the real part of the refractive index and not the absorptive part. The reflectance might be total under two different conditions: whenever $k >> n$ and near a longitudinal mode, where $\varepsilon(\omega) = 0$ and hence $n = 0$. There are cases, however, where the finite slab has virtually no absorption, so that its extinction coefficient is small. This is the case for a pure, high resistivity semiconductor at wavelengths far from its gap and its lattice absorption.

Apart from this simple behaviour, more complicated behaviour at interface must be included; light may be reflected and transmitted at the back surface, giving rise to a possible interference situation between light reflected from the back surface with those reflected from the front surface.

In such a situation reflectance and transmittance yield a phase term related to the beam travelling through the film, and transmittance becomes

$$T = \frac{(1-R)^2 e^{-\alpha d}}{1 - R^2 e^{-2\alpha d}} \tag{2.15}$$

where R is the reflection from the front surface of the slab and $\alpha = \frac{2\omega k}{c} = 4\pi q k$ is the absorption coefficient , q being the wavenumber of the radiation. If the transmittance is measured and the front reflectance and the thickness are known, α can be found from the above equation. Equation (2.15) shows how the intensity transmitted through the slab is affected both by the front surface reflectance and by exponential loss, the latter accounted by the exponential term.

In the limit in which the front and back surface reflections are negligible ($R = 0$), the transmitted intensity I_t is related to the incident I_i intensity by

$$I_t = I_i e^{-\alpha d}, \tag{2.16}$$

showing that the absorption coefficient α is the fractional change in intensity per unit length of penetration, due solely to absorption. This direct connection to physical

processes makes α a very useful spectroscopic quantity. Since the absorption is often proportional to the concentration of the absorbing entities N, a helpful absorption cross-section $\sigma = \alpha/N$ can be defined. This scenario is the most appropriate for the samples in our study.

Another useful form for equation (2.16), relating to the region of the sample probed by optical radiation is the so-called "penetration depth"

$$I_t = I_i e^{-\frac{z}{\delta}} \tag{2.17}$$

where the quantity $\delta = 1/\alpha$, is the penetration depth and is the distance over which the incident light falls to $1/e$ of its value at the surface. This quantity depends on frequency and on the semiconductor parameters through the dependence of α on such quantities. In the middle and far infrared (IR), the strongest absorption likely to be encountered is ~ 10^4 cm^{-1} and hence infrared radiation generally penetrates a distance of the order of 1μm or greater. Thus for most semiconductor dielectric layers and microstructures, whose thickness rarely exceeds a few μm, the light will sample throughout the entire depth of the layer. Hence IR spectroscopy cannot be considered in general as a surface-sensitive technique (in the way that XPS or SIMS are surface sensitive, ~ 30 - 150 nm sampling depth [2]), although variations on the basic arrangement, such as attenuated total reflection (ATR), enable greater surface sensitivity [3]. Infrared analysis in the form presented above probes the entire region of such layers. This lack of high surface sensitivity will hinder the study of very thin layers and surface localised species and the motivation of this work was to examine whether the effects of plasma etching were visible by standard FTIR spectroscopy.

2.3: Details of vibrational spectroscopy

IR spectroscopy is particularly important because of the high information content of a spectrum and because of its ease of sample preparation and measurement.

Infrared radiation can interact with the vibrational and rotational motion of molecules thereby giving information about systems of molecules. A necessary requirement for interaction between the IR radiation and the molecules is that a change in the molecular dipole moment occurs. In such a way one can obtain information about vibrational spectra of molecules. It is clear that electromagnetic radiation can interact with a moving charge such as an electron and that energy can be absorbed by it. Likewise, a vibrating or rotating atomic group can be associated with the motion of an electric charge, when the charges in a molecule are asymmetrically distributed or when the charge distribution becomes asymmetric by the vibration of the atoms. Consequently, a molecule can absorb electromagnetic radiation of a frequency corresponding to its vibrational frequency if a change in the dipole moment is associated with vibrational excitation of the atomic group concerned. Diatomic molecules with the same atoms, for example are not vibrationally excited by electromagnetic waves in a first order approximation, because they don't have any net dipole moment. Molecules consisting of various dissimilar types of atoms, however, can always interact with infrared radiation due to their intrinsic dipole moment. Vibrations showing no change in the dipole moment are characterized as infrared inactive [4]. It should be noted however that in a higher order of approximation, even in diatomic molecules with the same atoms, a dipole moment can be excited by nuclear vibrations, and these moments can then interact with electromagnetic fields, leading to weaker but observable effects.

In a spectrometer the molecule is irradiated with a whole range of infrared frequencies but it is only capable of absorbing radiation energy at specific frequencies that match the natural vibrational frequencies of the molecule. These normally occur in the infrared region of the electromagnetic spectrum (wavelengths of ~10 – 100μm). While the absorption frequency depends on the molecular vibrational frequency, the absorption intensity depends both on the molecular density and also on how effectively the infrared photon energy can be transferred to the molecule. This in turn depends on the dipole moment of the molecule. The dipole moment, in the simplest case of two charges, is defined as the magnitude of either charge in the dipole multiplied by the charge spacing

$$\vec{\mu} = q \cdot \vec{r} \tag{2.18}$$

A molecule that has no center of symmetry has in general an electric dipole moment, and this is given by

$$\vec{\mu} = \sum_i q_i \cdot \vec{r}_i \tag{2.19}$$

where the summation involves all the positive and negative charges of the molecule, and $\vec{r}_i$ are the positions of the charges. Since the wavelength of infrared radiation is much greater than the size of most molecules, the electric field of the photon in the vicinity of a molecule can be considered uniform over the whole molecule. The force exerted by the electric field on the molecular charges acts in opposite direction on opposite charges. Therefore the spacing between the proton and the electron centres of charge will tend to change inducing the dipole moment of the molecule to oscillate at the frequency of the photon. The more the dipole moment changes during a vibration, the more easily the photon electric field can activate that vibration. Detailed selection rule show that in order to absorb infrared radiation, a molecular vibration must cause a change in the dipole moment of the molecule. It can be shown that the intensity of an infrared absorption band is proportional to the square of the change in dipole moment, with respect to the change in the normal coordinate $(\frac{\partial \mu}{\partial Q})^2$ of the molecular vibration, giving rise to the absorption band. If in the molecule has a centre of symmetry at equilibrium, and this is retained during the stretching vibration, this vibration will be symmetric with respect to the centre of symmetry and infrared inactive [5].

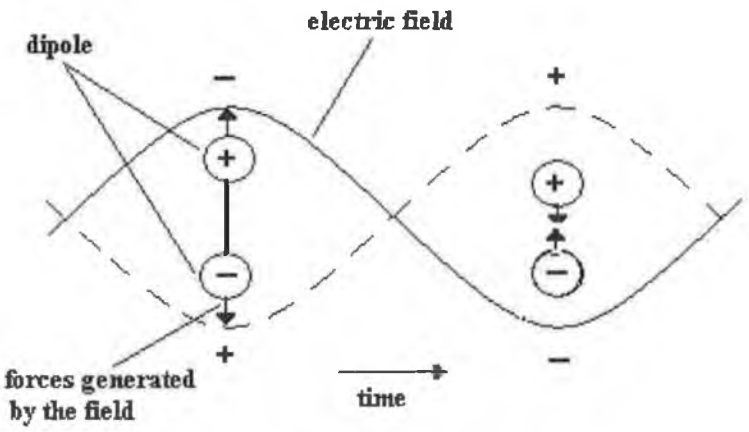

Figure 2.2: The forces generated on a dipole by an oscillating electric field alternately increase and decrease the dipole spacing

2.4: Types of molecular vibration

In the simplest case of a diatomic molecule only one single vibrational mode can be performed. For multi-atomic molecules [4], the number of possible vibrational modes can be calculated as follows: each single atom can move in three spatial directions corresponding to 3N spatial coordinates for N number of atoms. Thus the whole system has 3N degrees of freedom available. However, in three of these degrees of freedom, the atoms do not shift relative to one another, but they all move in the same direction, thereby changing the position of the center of mass. Additionally, three other degrees of freedom cause a rotation around the center of mass, so that the actual number of degrees of freedom of the molecule is

$$Z = 3N - 6 \tag{2.20}$$

Linear molecules, however, have only two rotational degrees of freedom, because the rotation around the molecular axis is not linked to any movement of the atoms or of the center of mass. Therefore this molecular type has one more degree of freedom

$$Z = 3N - 5 \tag{2.21}$$

The number of vibrations calculated above is called the molecule's normal modes of vibration, which can be excited independently from one another. The atoms involved in these normal modes oscillate with the same frequency and move in phase relative to each

other. Each normal vibration will have a particular vibrational frequency, and generally different vibrational modes will not have the same frequencies.

The names assigned to the common types of vibrational motions that can be observed in molecules (shown in figure 2.3 below), are:

-stretching vibrations

a. symmetrical
b. asymmetrical

-bending vibrations

a. in plane vibrations
    - rocking
    - scissoring
b. out of plane vibrations
    - wagging
    - twisting

The vibrations of groups of atoms in a larger solid matrix (such as bonded Si and O atoms in an amorphous SiO_2 structure) behave similarly to isolated molecules and show similar order of magnitude values for vibrational frequencies and the vibrational modes are labelled in the manner outlined above.

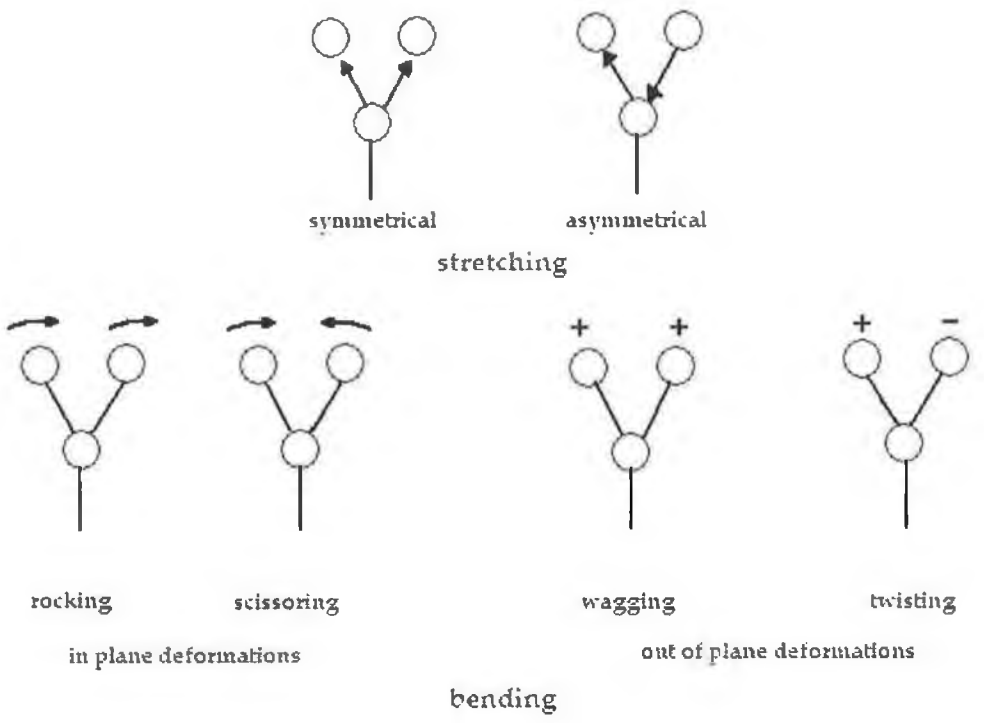

Figure 2.3: Schematic representation of molecular vibrations for triatomic molecules

References

[1] S. Perkowitz "Optical characterization of Semiconductors: Infrared, Raman, and Photoluminescence Spectroscopy", Academic Press, 1993.

[2] Xi Li, Li Ling, Xuefeng hua, Masanga Fukasawa, Gottlieb S.Oherlein, " Effects of Ar and O_2 additives on SiO_2 etching in C_4F_8-based plasmas", J.Vac.Sci.Technol.A21(1), Jan/Feb 2003.

[3] Sang M.Han, Eray S.Aydii, "Structure and chemical composition of fluorinated SiO_2 films deposited using SiF_4/O_2", J.Vac.Sci.Technol. A15 (6), Nov/Dec 1997.

[4] H.Gunzler, H.U. Gremlich "IR spectroscopy- an introduction", Wiley-Vch, 2002.

[5] N.B.Colthup, L.H.Daly, S.E. Wiberley "Introduction to infrared and Raman spectroscopy", Academic Press Inc., 1990.

CHAPTER 3: OVERVIEW OF PLASMA ETCHING AND RADIOFREQUENCY DISCHARGES

3.1: Introduction

Plasma-based surface processes are a relatively new technique in manufacturing very large scale integrated circuits [1]: introduced in the seventies mainly for stripping resists, they have over the last 15 years rapidly developed in the microelectronic industry and particularly found use in the fabrication of silicon integrated circuits. In this field, plasma processing has become a powerful technique to etch layers. Nowadays many of the deposition and etching process steps involved in several technologies of integrated circuit fabrication are based on the chemistry and physics of plasmas instead of chemical processes as was the case around 20 years ago [2].

Among the several plasma etching methods, radio frequency (RF) plasma-based etching is one of the most important processing technologies used in the manufacture of highly integrated electronic circuits.

3.2: General overview on theory and concepts about plasma

A plasma is a partially ionised gas in which free electrons collide with neutral and ionized atoms/molecules. Ionized species are created and destroyed through collisions when an electron can be dissociated from neutral species or recombine with ionized species. Depending on the energy of the particles, collisions can result in various species, such as negative ions, excited molecules, neutral atoms and ions. A general feature of plasmas is overall electrical neutrality: any charge imbalance would result in electric fields that would tend to move the charges in such a way as to rapidly eliminate the imbalance.

3.2(a): Electron distribution function

Because electrons play such an important role in plasmas, it is useful to categorize plasmas by electron densities and electron energies. Since the electrons in plasma have a distribution of energies, it is more correct to speak about average electron energies [2]. Generally electrons display a Maxwellian distribution of energies, which can be described in terms of the electron energy ε as

$$f(\varepsilon) = 2(\varepsilon)^{1/2} / ((\pi)^{1/2} (kT)^{3/2}) \exp(-\varepsilon / kT) \tag{3.1}$$

where $f(\varepsilon)$, the electron energy distribution function, is proportional to the number of electrons having an energy between ε and $d\varepsilon$, k is Boltzmann's constant, and T is the electron temperature. The electron energy is given by $\varepsilon = (1/2)mv^2$ where m is the electron mass and v is the magnitude of the electron velocity. The constants in equation 3.1 are such that the integral is normalized over all the energies

$$\int f(\varepsilon) d(\varepsilon) = 1 \tag{3.2}$$

and the average energy is obtained by the integral

$$\int \varepsilon f(\varepsilon) d(\varepsilon) = (3/2)kT \tag{3.3}$$

Thus the electron temperature T measures the average energy of the electrons for a Maxwellian distribution. A convenient unit for the electron temperature is the electron volt (eV) which is equivalent to a temperature of approximately 11600 K. The process plasmas of interest in the microelectronic industry have electron densities in the range of $10^9 - 10^{12} cm^{-3}$, and average electron energies between 1 and 10 eV.

3.2(b): Debye shielding

Even though there are different kinds of plasma depending on constituent atoms or molecules, densities, energies, degree of ionization, there is a basic feature common to all plasmas: the free charges in the plasma will move in response to any electric field in such a way to decrease the effect of the field itself. To understand this effect it is useful to bear in mind that the electrons, much lighter than ions, respond with high mobility to the electric field. This is why one can adopt a simplification in which the ions are stationary.

A straightforward implication of this is that electrons have a tendency to decrease the electric field since they respond quickly to any charge imbalance which creates an electric field so that there are no large regions with excess of either positive or negative charge. This feature is called as *quasi-neutrality*.

If an electric field is imposed on a plasma, the plasma electrons will distribute themselves in such a way as to diminish the effects: this phenomena is called Debye shielding. To explain this quantitatively we can examine the case of a positive test charge Q in a quasi-neutral plasma with equal electron and ion density which we call n. The electric potential that the charge would produce in isolation is

$$V_0 = Q/(4\pi\varepsilon_0 r) \tag{3.4}$$

where r is the distance from the charge and ε_0 the permittivity of the free space . But the total potential V includes the effects of the plasma electrons and ions, along with the test charge, and is given by the Poisson's equation

$$\nabla^2 V = -\rho/\varepsilon_0 \tag{3.5}$$

being ρ the total charge density in the plasma. The charge density is

$$\rho = e(n_i - n_e) + Q\delta(r) \tag{3.6}$$

where $\delta(r)$ is the Dirac delta function specifying that Q is a point charge, and n_i is the ion density, which, since the ions are immobile, can be taken as equal to n. The potential V in equation 3.6 will cause an alteration in the electron density, since the electron can move under the existence of such electric field. Using an electron density distribution

$$n_e = n\exp(eV/kT) \tag{3.7}$$

with the simplification $eV/kT << 1$ the Poisson's equation can be rewritten as

$$\nabla^2 V = -(en/\varepsilon_0)(1-1-(eV/kT)) + Q\delta(r) \tag{3.8}$$

having a solution

$$V(r) = (Q/4\pi\varepsilon_0)\exp(-r/\lambda_D^2) \tag{3.9}$$

where the quantity λ_D is called Debye length and is given by $\lambda_D = ((\varepsilon_0 kT)/(ne^2))^{1/2}$.

The plasma thus modifies V_0 from its free space value by attenuating it exponentially with a characteristic decay length of λ_D. This effect is called Debye shielding and describe how a plasma responds to an electric field: the electrons will collect in the vicinity of the test charge to screen its effect. Since the shielding decays exponentially, it can be quantified by calculating the number of electrons N_D in a sphere of radius λ_D called Debye sphere

$$N_D = (4\pi/3)\lambda_D^3 n. \tag{3.10}$$

For the plasmas of interest in the etching processes the relevant range of λ_D is from 0.01mm to 1mm, with 0.1mm being a good average for weakly ionised planar discharges. The value of N_D varies from about 10^4 to 10^7. One may thus say that within the bulk plasma the ions are not influenced by any imposed electric fields and move randomly (because of Debye shielding).

3.2(c): Reaction rates

When radicals and ions are formed, they can also undergo further reactions, often at high rates, to form additional chemically reactive species. The rates, κ, with which chemical reactions are activated is of the form

$$\kappa = A\exp(-B/RT) \tag{3.11}$$

where A is a pre-exponential factor, B is the activation energy for the reaction, R is the universal gas constant and T the absolute temperature. That means that for a reaction in which A and B are given the rate depends only on the temperature.

3.3: Plasma characteristics and generation

To form and maintain a plasma state requires an energy source to produce the required ionisation: the rate of ionization in a steady state must balance the losses of ions and electrons from the plasma volume by recombination and diffusion in the chamber. A widely used method for generating and sustaining a plasma [3] is by using an electrical breakdown of a neutral gas in the presence of an external electric field. In fact, any

volume of a neutral gas always contains a few electrons and ions: these free charge carriers are accelerated by the electric field and new charged particles may be created when these charges collide with atoms and molecules in the gas or with the surfaces of the electrodes generating the electric field. This situation leads to an avalanche of charged particles that is eventually balanced by charge carrier losses, so that a steady-state plasma develops. The types of plasmas involved in the microelectronic industry are initiated and sustained by electric fields which are produced by either direct current (dc) or alternating current (ac) power supplies. There can be several types of discharges, such as dc discharges, ac discharges, and pulsed discharges depending on the temporal behaviour of the electric field. The typical ac frequencies of excitation are 100 kHz, at the low end of the spectrum, 13.56 MHz in the RF portion of the spectrum, and 2.45 GHz in the microwave region. Such plasmas are also referred to as *electric discharge*, *gaseous discharge*, or *glow discharges*, respectively. In the collisions generated by the electric field between electrons and ions the electrons retain most of energy because of their small mass and transfer this energy mainly in inelastic collisions. Thus the electrons and ions may have significantly different temperatures, which give the plasma unique physical and chemical properties.

3.4: RF discharges and etching

The main type of discharge used for technical and industrial applications are radio-frequency (RF) discharges, in which a high-frequency electric (or electromagnetic) field is present. This is the case in our experiments, in which a capacitively coupled RF plasma tool was used. Capacitively coupled RF plasmas are the most common plasmas used in dry etching [1], and they are characterized by the presence of a capacitor between the electrode and the power generator and a matching network to adapt the impedance of the power generator to that of the discharge [3]. A conventional reactive ion etching (RIE) system is shown in figure 3.1. The material to be etched is placed on the RF-driven electrode inside a vacuum chamber. An RF power source is applied to the electrode or in some special cases it might be applied to the reactor walls.

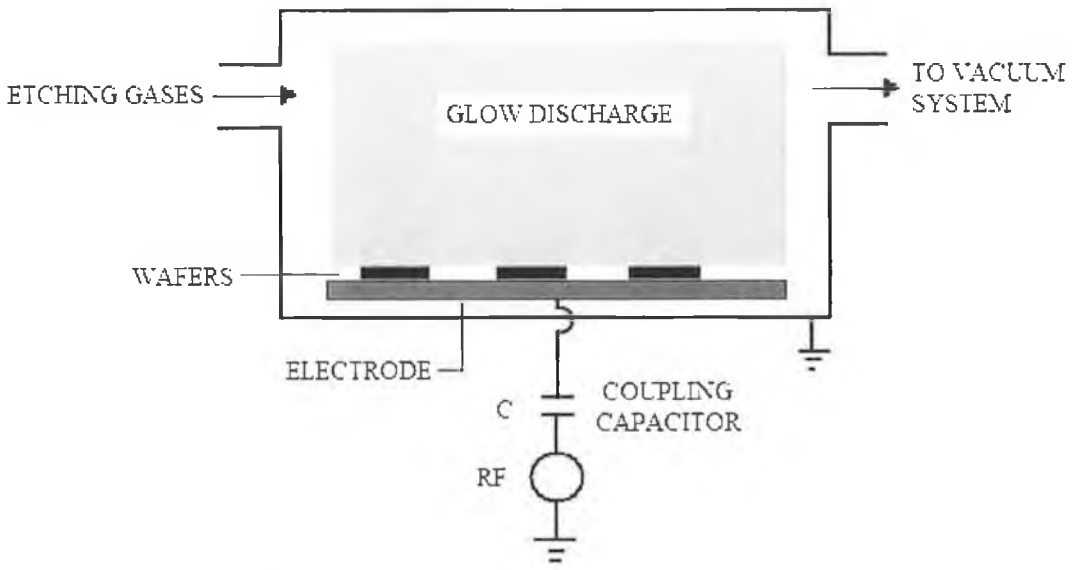

Figure 3.1: Schematic representation of simple capacitively coupled RF plasma etch reactor [3]

Inside the chamber, the mobile plasma electrons respond to the instantaneous electric field produced by the RF driving voltage (figure 3.2), oscillate back and forth within the positive space charge of the ions. The electrons also have far higher thermal velocities than the ions due to their smaller mass. On the contrary the ions, because of their mass, respond only to time-averaged electric fields and have smaller thermal velocities. The electrons tend to thermally diffuse to the capacitively-isolated electrode faster and hence charge it negatively. This creates a sheath layer close to the electrode with an electric field directed towards the electrode which equalises the ion and electron current to the electrode in steady state. Hence, ions flowing out of the bulk plasma near the centre of the discharge can be accelerated by the sheath field to high energies as they impinge on the substrate, leading to energetic-ion enhanced processes and reactions at the surface.

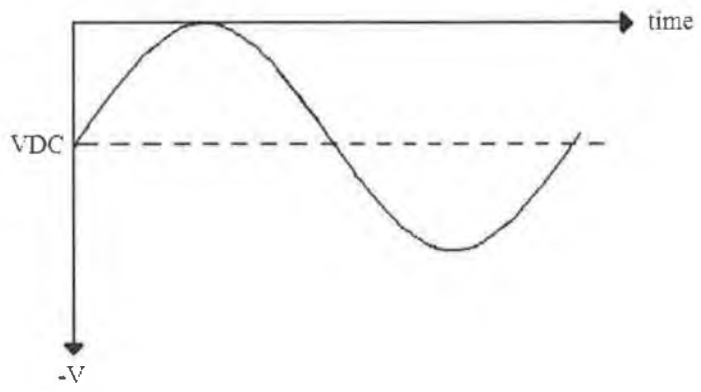

Figure 3.2: DC and AC voltage of the powered electrode: the DC voltage superimposed to the RF driving voltage is a direct consequence of the capacitor coupling the AC power source and the electrode

The reactions occur with the unmasked areas of the wafer and lead to the formation of volatile products, which enter the gas phase. Thus, reactive ion etching (RIE), which is a dry etching technique, is substantially characterized by the fact that it combines physical sputtering with the chemical activity of reactive species.

A schematic summary of the processes taking place in the system during reactive ion etching are the followings [2]:

- Active species generation: electron-impact dissociation/ionisation in a glow discharge (with a suitable feed gas, e.g. C_4F_8 in the case of silicon and silicon dioxide) is used to generate the gas phase etching environment which consists of radicals, positive and negative ions, electrons, and neutrals.
- Formation of a dc bias for ion acceleration. The material to be etched is placed on the high-frequency-driven (13.56 MHz) capacitatively coupled electrode. Since the electron mobility is much greater than the ion mobility, after ignition of the plasma the electrode acquires a negative charge (the corresponding voltage is called self-bias voltage). Therefore, the electrode and material placed on the electrode will be exposed to energetic, positive ion bombardment.

- Transport of plasma-generated reactive intermediates from the bulk of the plasma to the surface of the material being etched: this occurs by diffusion and influences the etch rate.
- Adsorption step: reactive radicals (e.g. F atoms) adsorb on the surface of the material (e.g. Si) to be etched. This step can be strongly enhanced by concurrent ion bombardment which serves to produce "active sites" since it aids in the removal of the surface layers which otherwise may passivate the surface.
- Reaction step: a reaction between the adsorbed species and the material to be etched must take place. In the case of fluorine-based etching of silicon chemical reactions between the fluorine atoms and the surface produces volatile species (like SiF_4 or SiF, SiF_2, SiF_3).
- Desorption of volatile reaction product: desorption of the reaction product into the gas phase is one of the most critical steps in the overall etching reaction. This removal can be greatly accelerated by ion bombardment via sputtering.
- Pump out of volatile reaction product: the desorbed species must diffuse from the etching surface into the bulk of the plasma and then be pumped out. Otherwise plasma induced dissociation of product molecules will occur and redeposition can take place.

Although all the physical and chemical processes underlying plasma etching are not completely understood yet, this technique meets some of the major technological requirements for processing, such as etch directionality (anisotropy) and selectivity [4]. The combination of physical sputtering and chemical reactivity for the case of SiO_2 enables a uniquely material selective anisotropic etch, as discussed further below. Etch anisotropy means the ability to remove material with a strong directionality: for example in deposition and pattern transfer the etch process has to remove material from the film leading to vertical sidewalls aligned with the resist mask (figure 3.3). This can be accomplished only if the etch process occurs in vertical direction only and the horizontal etch rate is zero so that sidewalls are unaffected and undercutting is minimal, enabling narrow feature widths. Etch selectivity on the other hand means the removal of only certain chemical species from the surface and is achieved as a result of chemical

reactions. It can be therefore seen that anisotropy and selectivity are, broadly speaking, in competition, since ion bombardment on the vertical direction removes material regardless of the chemical composition or percentages. The ability of RIE to meet both these goals underlies its technological dominance.

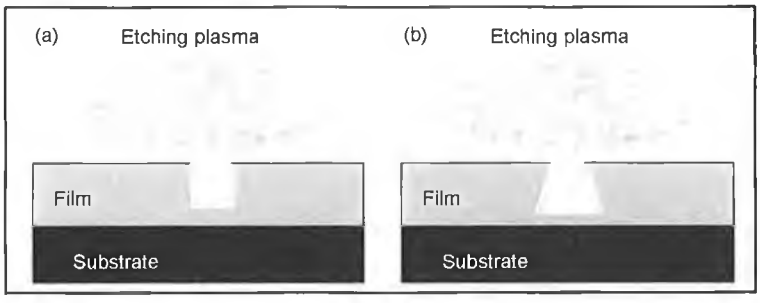

Figure 3.3: Schematic diagram of RIE process, showing (a) anisotropic etch with vertical sidewalls and minimal undercutting and (b) isotropic etch with substantial undercutting

The particular mechanisms by which RIE can enable both anisotropic etching and etch selectivity for the case of the etching of SiO_2 depends on the details of the plasma parameters. This anisotropy may be enabled in at least two ways. Firstly, ion bombardment may enhance the local etching rate. While the etch mechanism itself is chemical in its nature, ion bombardment may play an important role in influencing the rate of etching. The adsorption of chemically reactive species may be enhanced by ion bombardment because the impinging ions might break a bond and form active sites that are more easily filled with reactive radicals. Additionally the incoming ion can also deliver the necessary energy to form bonds between atoms on the wafer surface and reactive radicals from the plasma (covalent bond between silicon and fluorine for example), or to rearrange fluorine and silicon atoms. Also, the product molecule remains initially at the surface of the substrate: it needs a certain minimum energy to be removed and this energy can be furnished by an incoming ion.

Secondly, in a related scenario, the plasma deposits a passivating polymer on the surface it interacts with. Since the feed gases suitable for etching on SiO_2 contain fluorocarbon compounds, the polymer is normally formed by C and H/or F atoms provided, resulting in a $C_xF_yH_z$ polymer. The formation of the polymer does not occur only on the wafer

actually, but on all the reactor surfaces (which can result in negative consequences such as redeposition of particulates that locally prohibit etching resulting in a rough surface or incomplete removal of the etched layer). The polymer is removed by sputtering in regions where the ions bombard the surface normally and the chemical etching can continue, whereas in the regions where the ions do not strike the surface (i.e. vertical sidewalls) the polymer is not removed and the chemical etching is impeded.

In most real scenarios both mechanisms and other, related, mechanisms are at work and the detailed values of the process parameters will determine which mechanism dominates. However, in both cases, since the bombardment only occurs on horizontal surfaces the etching is only enhanced / enabled on such surfaces, resulting in an anisotropic etching. This is shown in figure 3.4 below.

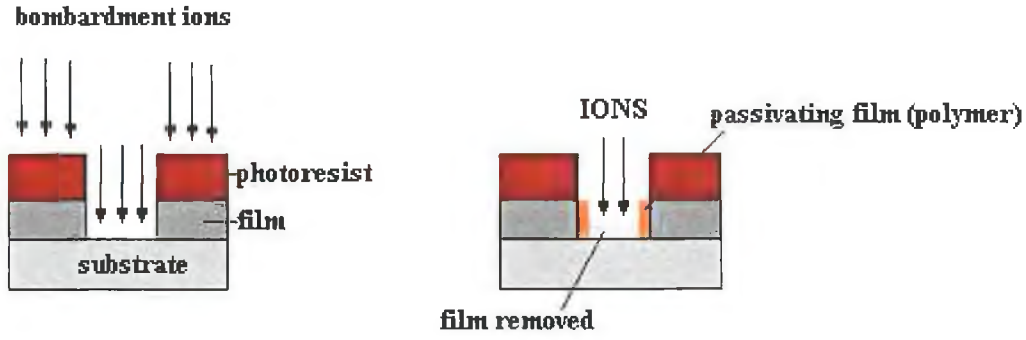

Figure 3.4: Example of a substrate with metal film and photoresist to show the role of ion bombardment: ions leaving the discharge bombard the bottom of the trench but leave the sidewalls unaffected, leading to anisotropic etching. (a) Either the ion bombardment increases the reaction rate at the surface, (b) or it exposes the surface to etchants removing passivating films that cover the surface

In general, as mentioned above, the actual etching is a chemical etching, not a physical, sputtering, one: a chemical reaction takes place between the solid atom (from the film to be etched) and gas atoms to form a molecule, which is removed from the substrate. Since a DC bias is always present, - as already seen-, there's always some sputtering but it

plays such a negligible role in directly etching the film material that it can be mainly neglected.

The main practical steps in the etching process are:

- formation of the reactive particle
- arrival of the reactive particle at the surface to be etched
- adsorption of the reactive particle at the surface
- chemisorption of the reactive particle at the surface with formation of chemical bond
- formation of the product molecule
- desorption of the product molecule
- removal of the product molecule from the reactor.

When the gases enter the reactor in the form of molecules, the molecules aren't reactive enough in most cases to react chemically with the surface. The ionization in the discharge dissociates the molecules into chemically reactive atoms (radicals).

Capacitively coupled RF plasmas have been utilized as the main tools for plasma etching thanks to the simplicity of manufacturing the reactors to generate these plasmas. But these types of plasma also have limitations. In particular the reactive particle density is strongly coupled to the ion energy, so that one can't achieve a high density of free atoms (the ones directly responsible for the etching since they react with the wafer surface atoms) without having a lot of ions with also high energy. This means that having highly chemically reactive plasma with little ion bombardment to attain a mainly chemical etching process is quite difficult. In addition it is not possible to generate plasmas at low pressures (10mTorr is typically the lowest at which the plasma can be sustained), a condition that would be required to obtain ions coming at nearly perpendicular angles (few collisions should take place to achieve this, resulting in a large mean free path) to achieve the best degree of anisotropy.

3.5: Plasma reactor tool used in DCU

In the experiments carried out for our analyses a Lam9100 dual-frequency plasma tool was used. In this tool (figure 3.5) a 13.56 MHz transformer coupled (TCP) source produces the plasma density, and a 4 MHz capacitive coupled (CCP) wafer platen electrode is used to develop the RF bias. As stated in the previous paragraphs plasma sources are usually operated with static or alternating electromagnetic field. When an additional magnetic field (as it is the case in the reactor in figure 3.5) is present this is done for two main reasons: firstly the plasma confinement is enhanced by limiting the diffusion of charged particles perpendicular to the magnetic field, secondly the power absorption is improved by increasing the electron-neutral collisions rate due to the longer trajectories of electrons.

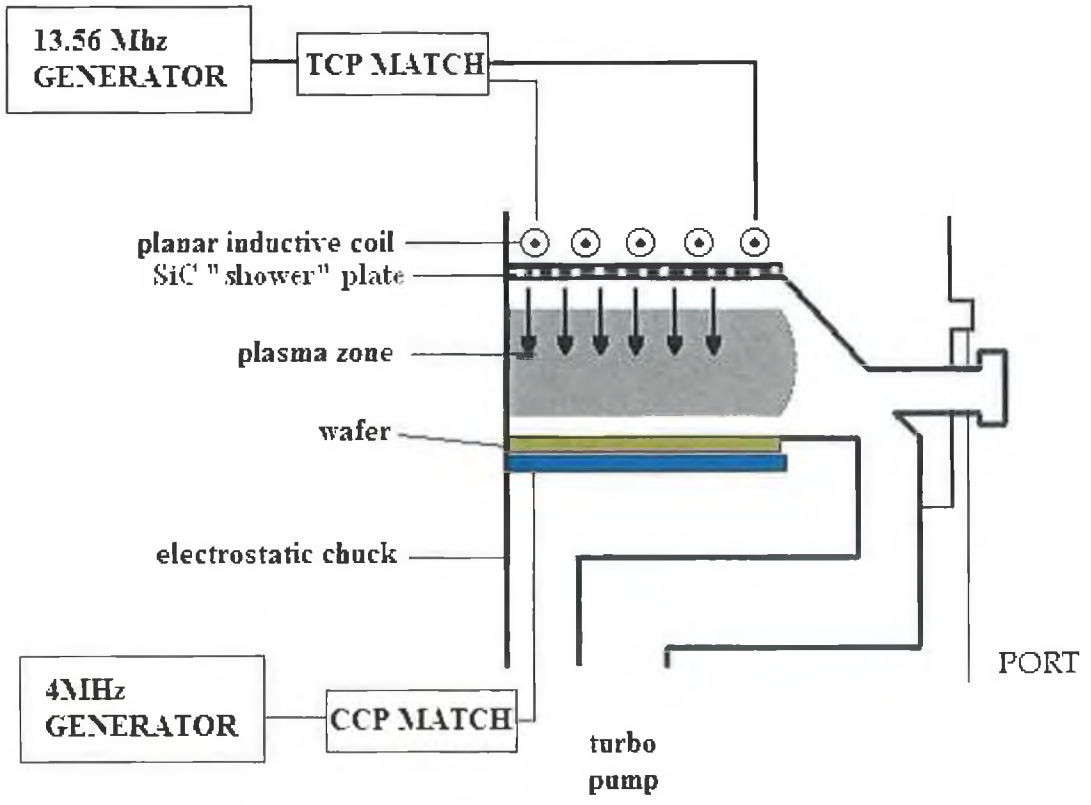

Figure 3.5: Lam9100 dual-frequency plasma-tool [5]

The possibility of a dual frequency permits the selection of an upper and lower power: the first one creates ions, the second one accelerates them, and hence one may control density and energy separately. The reason for having a dual frequency reactor is that having only one frequency it wouldn't be possible to control both the density of the ion flux (current) impinging on the wafer surface and the ions' energy: at low pressures such as the ones involved (ranging from15mTorr up to 45mTorr) it wouldn't be possible to create a dense plasma by other methods. Ordinary plasma sources give an ionization fraction of roughly 10^{-6}, while using a TCP source increases the ionization degree up to 10^{-4}.

The TCP source is the one operating at a frequency of 13.56MHz, while the CCP source operates at 4MHz; each of them has typical RF power ranging from 600-1200W (*upper power*) and 200-600W (*lower power*) respectively. The upper power level controls the ionised particle density (higher upper power means high ion density) while lower power controls the ions' energy impinging on the surface (higher lower power means more energetic ions impinging on the sample's surface). Basically the 4MHz CCP signal enables independent control of the sheath layer mentioned previously. Changing the value of the CCP power affects the energy with which electrons and ions strike on the wafer surface. These energies are of the order of tens of eV.

Finally, it is necessary to explain the reason why a SiC plate shower is used. The feed gases are not conveyed into the chamber through a tube, but through the very small holes (∅<1mm) of the SiC plate. SiC is a good material for this purpose for two main reasons:

- It has high chemical resistance, so that it doesn't contaminate the sample surface;
- Is a dielectric for direct currents but a very good conductor at high frequencies, so that it doesn't absorb the RF discharge.

References

[1] M.A. Lieberman, A.L. Lichtenberg, "Principles of plasma discharges and materials processing", John Wiley and Sons, 1994.

[2] Rossnagel, Cuomo, Westwood, "Handbook of plasma processing technology: fundamentals, etching, deposition, and surface interactions", Noyes Publications, 1989.

[3] H. Conrads, M.Schmidt, "Plasma generation and plasma sources", Plasma Source Sci. Technol.9 (2000),441-454.

[4] Gottlieb S. Oehrlein, Holly L. Williams, "Silicon etching mechanism in CF_4/H_2 glow discharge", J.Appl.Phys.62 (2), 15 July 1987.

[5] V.Krastev, I.Reid, G.Hughes, L.Oksuz, B.Ellingboe, A.Isliakin, V. Milosavljevic " Investigation of space variables in C_4F_8 /Ar/O_2, in press, J. Mat. Sci.

CHAPTER 4: FTIR; THEORY AND EXPERIMENTAL SET-UP

As already stated in Chapter 2, the importance of infrared radiation is due to the occurrence of infrared absorption by the vibrations associated with chemical bonds in a material. Chemical structural fragments within molecules, called *functional groups*, tend to absorb infrared radiation in the same wavenumber range regardless of the structure of the rest of the molecule to which the functional group belongs. This correlation allows the structure of unknown molecules to be identified from the molecule's infrared spectrum. This is why infrared spectroscopy is a useful chemical analysis tool.

4.1: FTIR operation

4.1(a): The interferogram

The key optical component of a Fourier Transform Infrared spectrometer (FTIR) device is an interferometer, usually based on the simple Michelson interferometer structure, figure 4.1, consisting basically of four arms: the first contains a source of infrared light, the second is a fixed mirror, the third is a moving mirror, the fourth is open and it is the one in which the sample and the detector are placed [1]. At the intersection of these four arms there is a beamsplitter, which transmits half of the radiation impinging upon it, and reflects the other half. As a result the intensity of radiation reaching the mirrors is half of the incident intensity, and, after reflecting off their respective mirrors, the two light beams recombine at the beamsplitter, where they interfere and then pass through the sample and are detected.

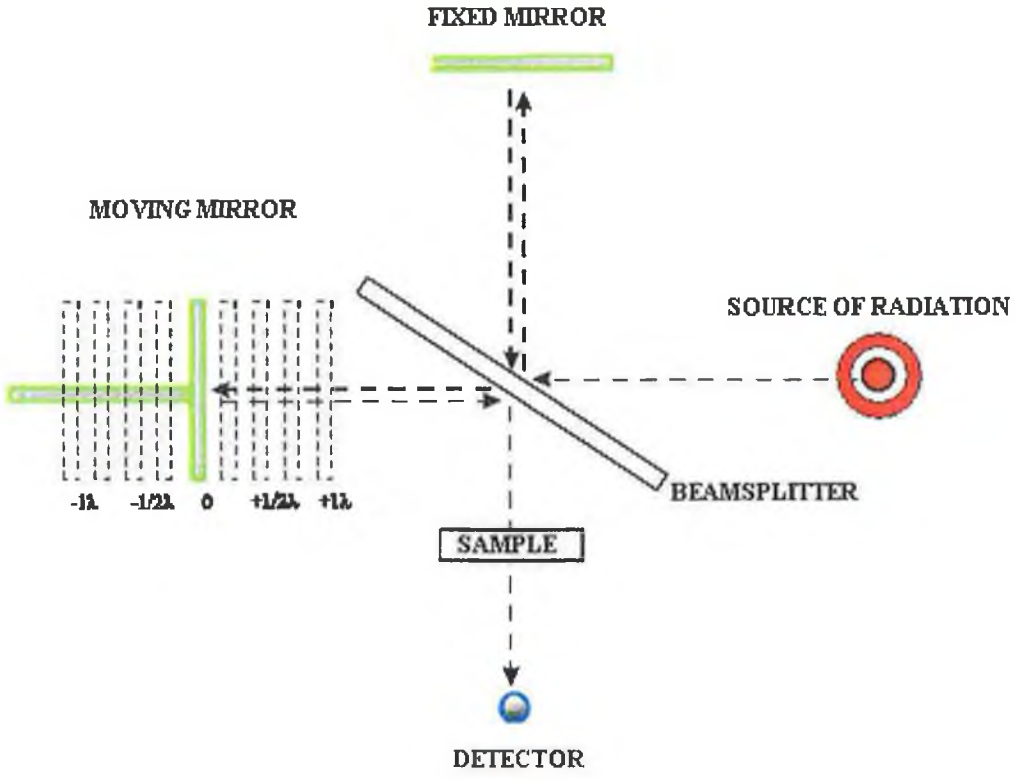

Figure 4.1: Schematic optical diagram of a Michelson interferometer [4]

The difference between the distances of the moving and the fixed mirror respectively from the beamsplitter is called the *path difference*; this difference is varied by translating the moving mirror away from the beamsplitter and vice versa. Depending on this path difference, the light waves that recombine at the beam splitter outlet may have yield destructive or constructive interference as shown in figure 4.2 (from ref.[1], pages 17 & 18). The condition for constructive interference is

$$\delta = n\lambda \tag{4.1}$$

while destructive interference occurs when

$$\delta = (n + 1/2)\lambda \tag{4.2}$$

with $n = 0,1,2,3,...$ in both cases.

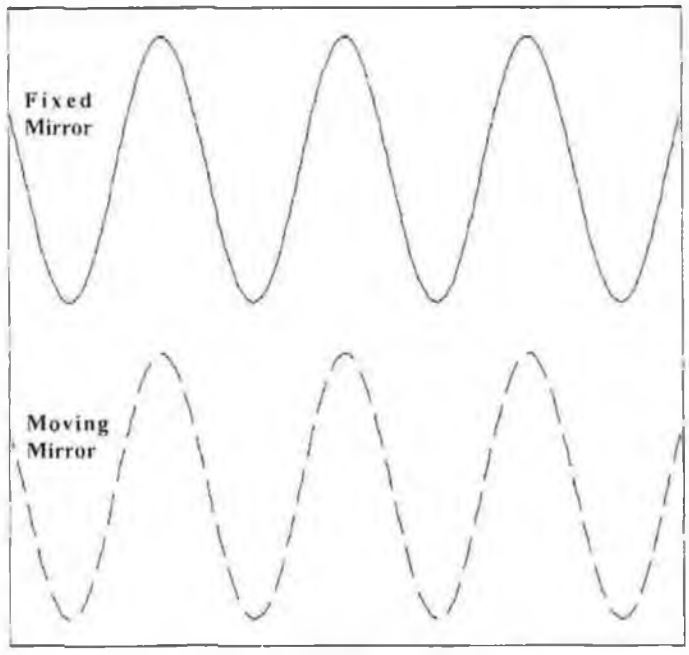

a)

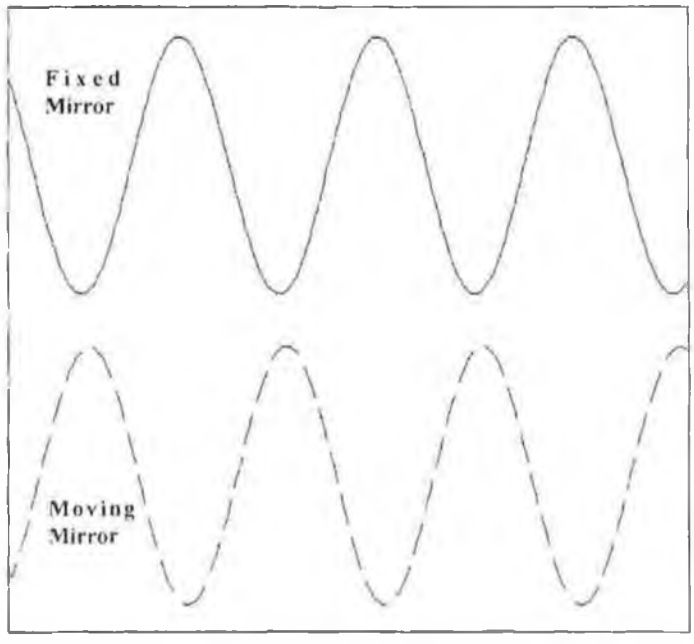

b)

Figure 4.2: Illustration of the electric fields (as a function of time) associated with the reflections from the fixed mirror and moving mirror in a Michelson interferometer with (a) zero path difference and (b) when the optical path difference is half of the wavelength of light

At optical path differences other than those given above, an intermediate interference condition is observed, and the light beam intensity is somewhere between maximum and zero. If the mirror is moved at constant velocity, the intensity of the infrared radiation varies smoothly. The variation of light intensity with optical path difference for a single wavelength source is measured by the detector as a sinusoidal wave and the plot of light intensity versus optical path difference is called *interferogram*. The interferogram is the fundamental measurement obtained by an FTIR and it is Fourier transformed to give a spectrum. This is where the term *Fourier Transform Infrared Spectroscopy* comes from. To generate a complete interferogram the moving mirror is translated back and forth over a certain distance once: this is called a *scan*. The constructive and destructive interferences that take place in the interferometer affect the light intensity as if a shutter was alternately blocking the beam and letting light trough. Therefore, the beam passing the interferometer is said to be modulated. This modulation occurs at a frequency is given by the following equation

$$F_V = 2VW \tag{4.3}$$

where F_V is the modulation frequency, V is the moving mirror velocity in cm/sec, and W is the wavenumber of the light in the interferometer measured in cm^{-1}. Equation 4.3 gives the frequency of the cosine wave interferogram that is measured by the detector for light of wavenumber W passing trough the interferometer. To get reproducible measurements on the same sample the frequency F_V must be reproducible: this is why it is important that the velocity of the moving mirror in an FTIR is accurately controlled.

Each different wavenumber of light gives rise to a sinusoidal wave signal of unique frequency that is measured by the detector. Interferogram signals are additive, so the actual signal measured by the detector will be the sum of all the contributions. In the case of the FTIR the source is generally a broadband infrared source, giving off light in a continuum of wavelengths, each of which gives rise to a different cosine wave interferogram whose frequency is given by equation 4.3. The total interferogram measured by the detector is the summation of all the interferograms from all the different

infrared wavelengths. The total interferogram is then Fourier transformed to give the spectrum back, as shown in more detail below.

4.1(b): Transforming the interferogram into a spectrum

As previously stated, when the moving mirror translates a retardation between the optical paths of the two arms of the interferometer (the ones with the mirrors) is introduced; the pattern of destructive and constructive interferences seen by the detector has a cosinusoidal variation

$$I(x) = B(\nu)\cos(2\pi x \nu) \tag{4.4}$$

In the above equation $I(x)$ is the intensity of the beam recorded at the detector, x is the moving mirror displacement in centimetres, and $B(\nu)$ represents the intensity of the source as a function of frequency ν in cm^{-1} [2]. However this equation refers to a monochromatic source. If we are dealing with a broadband source (Figure 4.3), using the same concept, we add (integrate) several monochromatic sources up to an infinite number of frequencies. The detector will now respond with an integration of the cosine waves associated to each frequency

$$I(x) = \int_{-\infty}^{+\infty} B(\nu)\cos(2\pi x \nu)d\nu \tag{4.5}$$

Equation (4.2) is nothing but the Fourier transform of the intensity of the source; since we are interested in the spectrum at the different frequencies we need to perform the inverse transform which changes (4.2) into

$$B(\overline{\nu}) = \int_{-\infty}^{+\infty} I(x)\cos(2\pi x \overline{\nu})dx \tag{4.6}$$

Equations (4.2) and (4.3) together define the relationship between the interferogram and the infrared spectra. Basically they show how the interferogram records the intensity of light as a function of the path difference, and then this function is mathematically Fourier transformed into a function of the frequency to give the infrared spectrum. The Fourier transform method mentioned is implemented in a computer using the Fast Fourier

Transform (FFT) algorithm, which can compute the Discrete Fourier Transform (DFT) faster than other available algorithms.

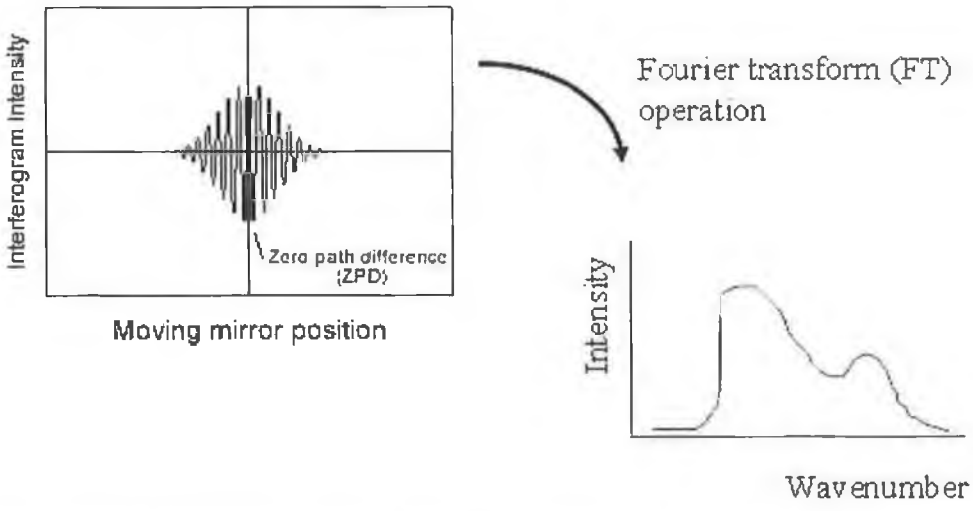

Figure 4.3: Schematic example of Fourier transformation relationship between interferogram and spectrum

The integral in equation 4.6 is over an infinite region, which would imply an infinite extent of mirror travel. Obviously the integral in equation 4.6 can be performed only over the distance that the mirror can travel. Mathematically this is expressed as a truncation of the interferogram $I(x)$ by a suitable truncation function. This truncation has two consequences.

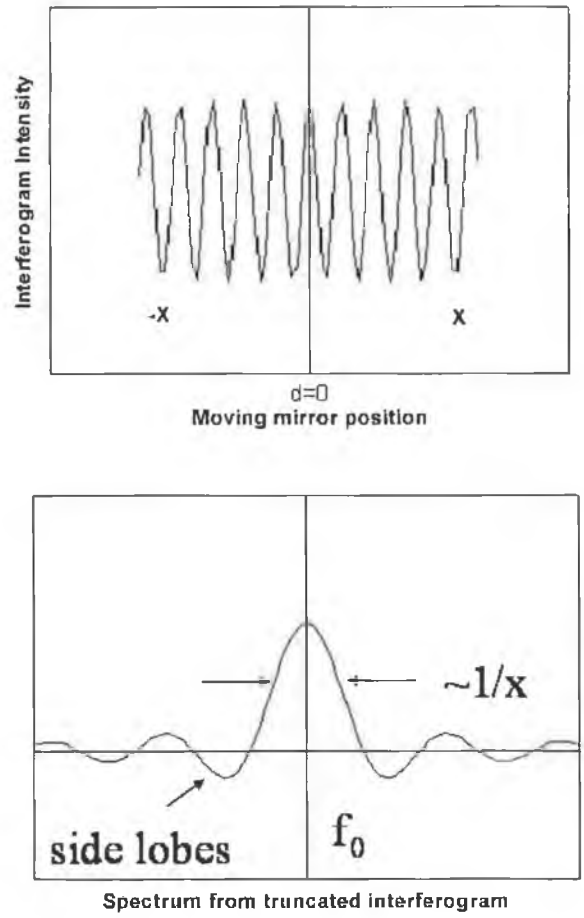

Figure 4.4: Example of spectrum calculated by inverse transformation of interferogram over total mirror travel distance x

Firstly, even if one uses a perfectly monochromatic source, the output spectrum is a broadened line, whose width is inversely proportional to the mirror travel distance x, as shown in figure 4.4 above. High-resolution information regarding the spectrum are those obtained from regions of the interferogram far from the ZPD. Two lines very close in wavelength will give similar interferogram patterns. If the mirror is moved only a short distance from the ZPD, it may not be sufficient for the FT spectrometer to detect each cosinuisoidal line, since the difference in wavelength becomes apparent the further the mirror moves. The total movement x of the moving mirror of the interferometer limits the resolution or band pass σ (in cm^{-1}) that can be realised. The resolving power R defined by $\lambda / \Delta\lambda_{min}$ is thus δ / λ where $\delta = 2x$ since

$$\Delta\left(\frac{1}{\lambda}\right)=\frac{\Delta\lambda}{\lambda^2}=\frac{1}{\delta} \tag{4.7}$$

Thus

$$R=\frac{\lambda}{\Delta\lambda}=\frac{\delta}{\lambda} \tag{4.8}$$

This means that for example a mirror movement of 5mm results in a resolving power of 20000 at a wavelength of 500nm and a resolution of 0.025nm.

Secondly, if the truncation is achieved with a sudden (box-car) function one sees the appearance of side-lobes around the major peak in the spectrum which could potentially mask other weaker signals in the same region. Thus it is necessary to truncate the integral by a mathematical function that smoothly reduces the intensity to zero at the mirror movement limit. Such function is called an apodisation function and it decreases the magnitude of the side lobes but at the expense of a slight loss of resolution (figure 4.5).

In summary, the resolution of a spectrum after performing a Fourier transform operation is ultimately dependent on the total distance that the travelling mirror can move and on the form of the apodisation function.

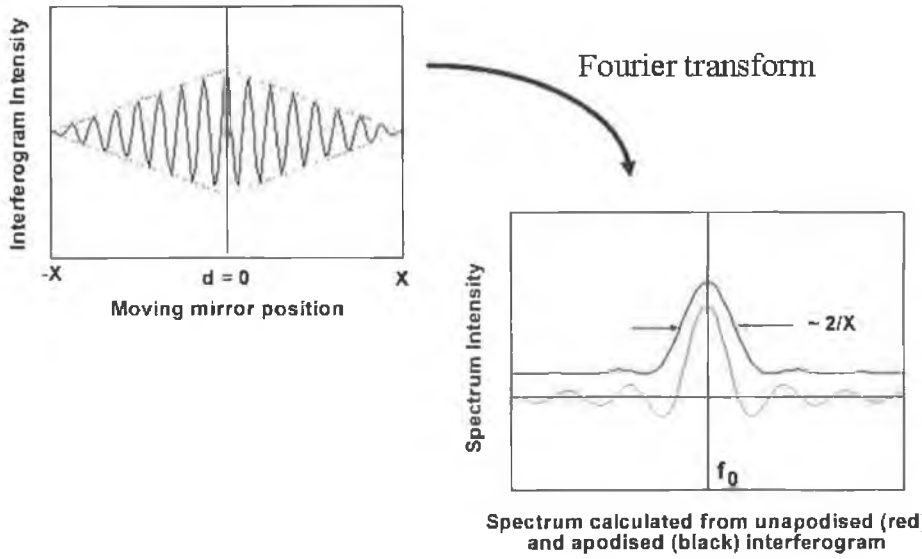

Figure 4.5: The apodisation function leads to a signifying loss of resolution; nevertheless, the line-shape of the spectrum is improved

When an interferogram is Fourier transformed, a single beam spectrum is obtained: in figure 4.6. A single beam background spectrum (i.e. obtained without a sample in the beam) is shown.

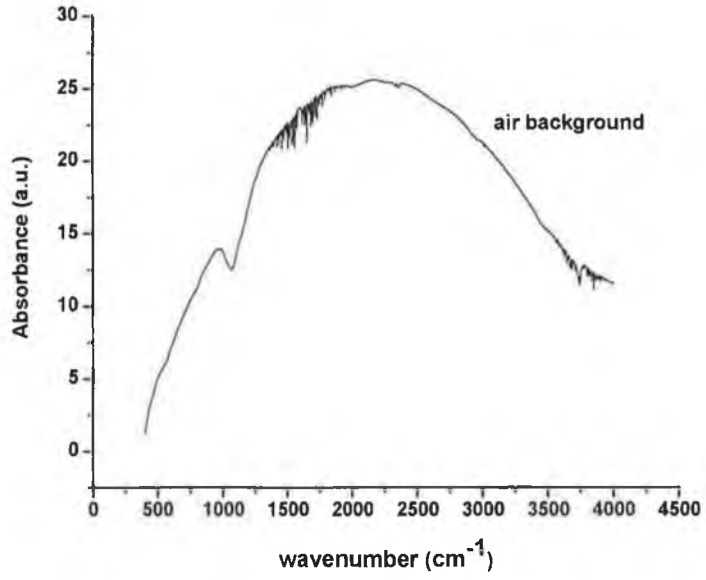

Figure 4.6: An example of a single beam background spectrum

It is always necessary to acquire a background spectrum against which the sample spectrum will be normalized in order to eliminate instrumental and the environmental contributions to the infrared spectrum of a sample [1].

The overall shape of this spectrum is due to the instrument response function: which is the convolution of the sensitivity of the detector, the transmission and reflection coefficients of the beamsplitter, the emissive properties of the source and reflective properties of the mirrors. Atmospheric water vapour and carbon dioxide inside the sample compartment are responsible for artefact features localized around 1630 cm^{-1} & 3500cm^{-1} and 2350cm^{-1}, respectively.

When the infrared beam passes through the sample and is Fourier transformed the sample absorption features are superimposed upon the instrumental and atmospheric contributions: to isolate these contributions the sample single beam is ratioed against the

background spectrum. This produces the real transmittance spectrum of the sample one uses the following equation

$$T(\%) = \left(\frac{I}{I_0}\right) x100 \tag{4.9}$$

where the percentage transmittance is the ratio between the intensity of light measured with a sample in the beam (I) and the intensity measured with no sample in the beam (I_0). Depending on the situation, one may choose to plot either the transmittance or the absorbance spectrum. The absorbance (A) can be derived from the transmittance spectrum using the following equation

$$A = -\log_{10} T \tag{4.10}$$

4.1(c): Advantages and limitations of FTIR

The main difference between Fourier transform spectroscopy and dispersive spectroscopy is that the intensity information at all the different wavelengths of light are contained in one measured interferogram (all the wavenumbers of light are detected at once): there is no need to physically separate the light beam into its component wavelengths and measure intensities one at a time as in dispersive spectroscopy. An immediate practical utility of this is that an FTIR can acquire a spectrum much faster than a dispersive instrument. On the other side, by adding interferograms together to get a spectrum, random noise is reduced and the signal-to-noise ratio (SNR) is improved: this process is defined *coadding*. Taking into consideration the SNR in a dispersive spectrometer (grating spectrometer) and assuming the noise is detector-noise limited, the noise for each spectral element will be proportional to the square root of the signal intensity; hence

$$SNR_{grating} \propto \sqrt{\frac{T}{N}} \tag{4.11}$$

Where T is the time for a hypothetical spectrum over a range ($\lambda_1 - \lambda_2$) to be taken and N the number of measurements (scans added together in the case of FTIR) required at a given resolution. In the case of FTIR, instead, since the spectrometer obtains an

interferogram, which is the result of all spectral elements, all the wavelength regions are examined simultaneously.

So that the integrated signal over the range ($\lambda_1 - \lambda_2$) is proportional just to the time

$$SNR_{FT-IR} \propto \sqrt{T} \tag{4.12}$$

Hence the ratio of SNR for FTIR spectrometer compared to that of grating spectrometer is

$$\frac{SNR_{FT-IR}}{SNR_{GRATING}} = \sqrt{N} \tag{4.13}$$

This is known as multiplex or Felgett advantage of FTIR [6].

Another advantageous aspect of FTIR is that the interferometer has a high optical throughput due to the circular entrance aperture. The resolving power R due to the aperture is

$$R = 2\pi / \Omega \tag{4.14}$$

where $\Omega = \pi \cdot (\theta/2)^2$ is the solid angle of admittance subtended by the source at the aperture (figure 4.7).

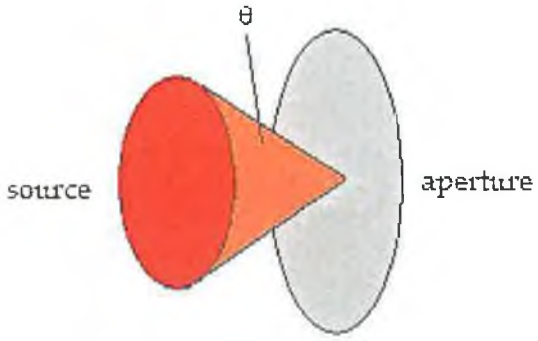

Figure 4.7: Definition of the angle of admittance

As the solid angle decreases (narrowing the aperture) the resolving power increases, but the amount of light entering the spectrometer is reduced. Thus, similarly to dispersive spectroscopy, FTIR has a trade-off between resolution and signal strength. Nevertheless, FTIR has a peculiar advantage, in term of throughput of light. In fact, the product of solid

angle of admittance and resolving power is usually at least one order of magnitude greater than for grating spectrometers [6]. This property is known as the throughput or Jacquinot advantage, and means that FTIR systems can operate at both high resolving powers and high signal levels simultaneously. This advantage is realised regardless of the wavelength region under examination or the detector being used.

Finally, another advantageous aspect of modern FTIR systems is the presence of the HeNe laser used to control the movement and the speed of the moving mirror for each scan which results in a more accurate and stable frequency calibration : this is called the Connes advantage.

However, a specific limitation of FTIR is that it is a single beam technique. As stated in the previous paragraph, this means that the background spectrum, which needs to be run before any sampling and that measures the contribution of the instrument and the environment to the spectrum, is measured at a different point in time than the spectrum of the sample. Ratioing the sample spectrum to the background spectrum ideally eliminates the instrumental and environmental contributions to the spectrum. Thus if something in the instrument or the environment changes between when the sample and the background spectra are obtained, spectral artefacts can appear in the sample spectrum. Examples of artefacts are water vapour or carbon dioxide peaks seen in figure 4.6.

4.2: Common FTIR system set-up

The main sections of an FTIR spectrometer can be summarized as (figures.4.8 and figure 4.9):

- **laser system** for control of distance and alignment;
- **interferometer** system based on the physics of a Michelson interferometer;
- **detector** for the transmitted light trough the sample.

The laser system consists of a HeNe laser that measures the distance between the scanning mirror and the beamsplitter depending on the triangulation method* of the reflected laser beam. The frequency-stabilised laser also acts as an internal wavelength reference for each scan. The He-Ne laser used in the DCU system (*Nicolet FTIR Nexus 470/670/870*) operates at a current of approximately 0.66A and emits at a frequency of 15798.260 cm^{-1}.

The modulated light passes trough the sample compartment and is focused upon the detector. The detector is simply an electrical transducer, and produces an electrical signal (voltage, resistance, or current) that is proportional to the amount of radiation striking it. It translates the incoming infrared light into an electric signal. The type of detector used in FTIR is a pyroelectric DTGS detector. A pyroelectric substance becomes electrically polarized when heated: the substance is electrically polarized in an electric field and retains residual polarization after the field is removed. This residual polarization is sensitive to changes in the temperature. The pyroelectric detectors are made from a thin single crystalline wafer of a pyroelectric material; the most common used being deuterated triglycine sulfate (DTGS). The changing degree of polarization upon exposure to the incoming IR radiation can be observed as a change in the electrical signal. The window of the detector is made of KBr and limits the measurements to the mid-IR region. The response time of this detector is fast and it can operate at room temperature. Being a thermal device, it possesses essentially flat response in the range of operation. The intensity measured with the detector is an output that is then processed by the computer software. Particularly, the instrument used in our analysis is a commercial *Nicolet FTIR Nexus 470/670/870* provided with an Ever-Glo mid-infrared source and DTGS-KBr detector coupled with a XT-KBr beamsplitter in the interferometer [3].

* It's called triangulation method because, as shown in fig.4.8, the distance between beamsplitter and moving mirror can be related to the distance between beamsplitter and the flat mirror using trigonometric formulas.

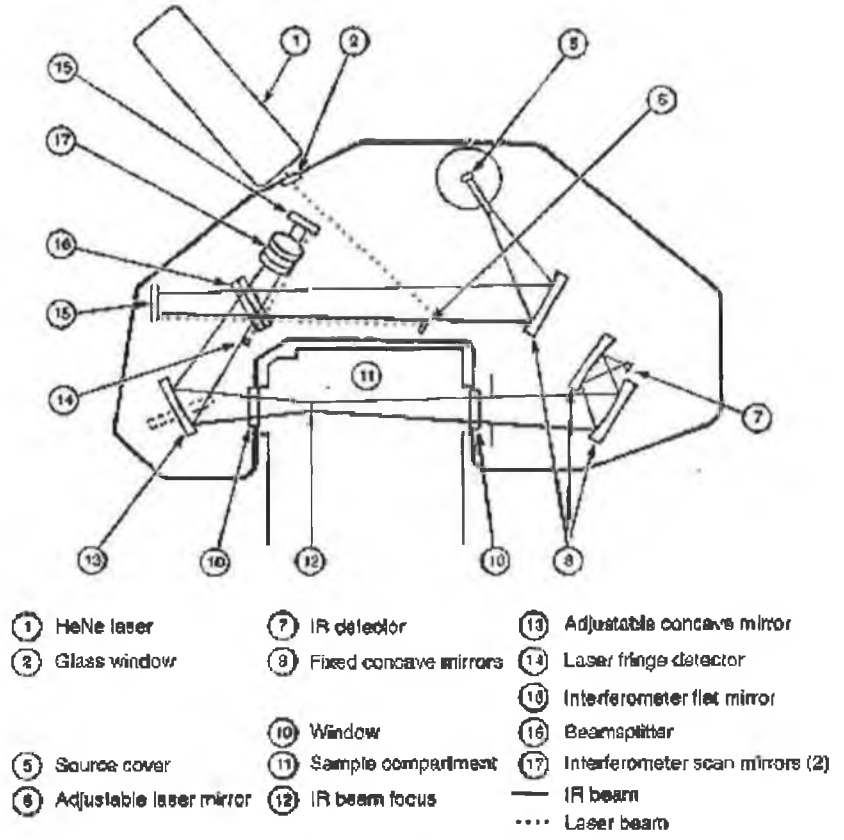

Figure 4.8: General schematic representation of the internal structure of an FTIR [4]

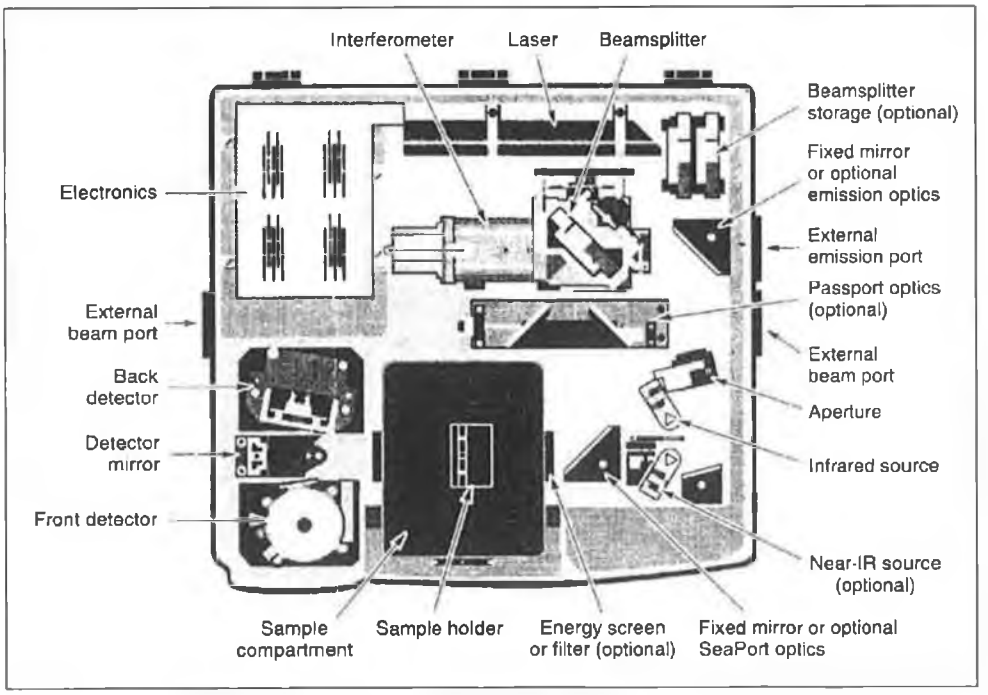

Figure 4.9: Inner view of Nicolet Nexus FTIR

The beamsplitter is selected in such a way that when is aligned the detector signal is as large as possible [3]. The coupling between these different components is always chosen depending on the range of investigation; in our analysis, whose range lies in the near-mid infrared (IR), the above combination is the most suitable. The coupling of the XT-KBr beamsplitter, the DTGS-KBr detector and the Ever-Glo source gives a total nominal spectral range (375-11,000) cm^{-1}: such a range reflects the combination of the Ever-Glo and white light sources, as well as the limits of the beamsplitter-detector combination. However, due to the convolution of beamsplitter and detector with the efficiency curve of the source, the spectral range at disposal is not as broad as the total, and lies between (400 - 4000) cm^{-1}. The Ever-Glo lamp operates at a nominal input voltage range of (8-11) V, but for better efficiency it is convenient to maintain the input voltage around 9.7-9.8 V. The system in controlled by provided commercial software OMNIC which automatically gives the plot of the optical quantity under examination (transmittance or absorbance) within the spectral range given by the system's specifications.

Since the possible presence of water vapour or air inside the sample compartment, figure 4.10, would affect the resulting spectra, figure 4.6, it is necessary to purge the sample department whilst performing the experiment. For this reason a purge gas that is free of moisture, oil and carbon dioxide is necessary. In our case, the choice is generally nitrogen, maintained at a pressure range of 20 to 40 psi.

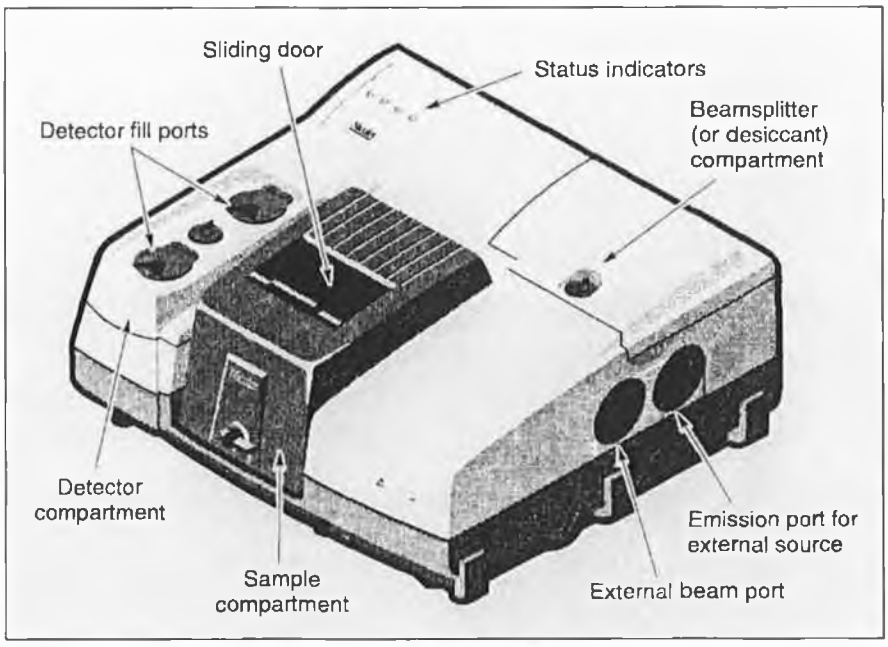

Figure 4.10: External view of Nicolet Nexus FTIR

4.3: Interpretation of IR absorbance spectra

We show below in figure 4.11 two examples of amorphous (a-) SiO_2 absorbance spectra (one taken from the literature (a) and one measured in our laboratory (b)). The sample used had an oxide thickness of ~ ~180 nm. Having acquired the spectra the first step is the identification of the spectral peaks. This may be done using spectral libraries or other literature sources. The spectra are taken and referenced to the background spectrum, that is to say the spectrum acquired with no sample in the infrared beam. In our case, the background spectrum was taken with a bare (i.e. very thin oxide layer, ~ 4nm) silicon sample.

Once the spectra are acquired, one may wish to calculate peak areas for certain peaks. In many cases individual peaks are superimposed on sloping or curved baseline and it is useful to correct such baselines with a baseline correction which will result in a spectrum with flat baseline prior to area calculations. Baseline corrections are performed by first generating a function that parallels the shape of the baseline; this function is then subtracted from the sample spectrum yielding a graph devoid of the curve or sloped baseline.

The next step is peak identification: here a first evaluation is needed to identify peaks that are not due to molecular vibrations in the sample, but are artefacts due to errors in the background (reference) spectrum. Common artefacts (mentioned previously) are due to incomplete elimination of the contribution of atmospheric water vapour and carbon dioxide inside the sample compartment, responsible for features localized around 1630 cm^{-1} & 3500cm^{-1} and 2350cm^{-1}, respectively.

For SiO_2, the characteristic features are shown in figure 4.11 consisting of four main absorption peaks centred respectively at ~ 457cm^{-1}, ~ 810 cm^{-1}, ~ 1076 cm^{-1}, ~ 1200cm^{-1}. The first one, having the lowest frequency, is associated with the rocking vibration of the oxygen atom about an axis through the two silicon atoms. The second peak is associated to the symmetric stretching of the oxygen atom along a line bisecting the axis formed by the two silicon atoms. The last two peaks are associated with asymmetrical stretching (AS) motion in which the oxygen atom moves back and forth along a line parallel to the axis trough the two silicon atoms. These two peaks can be thought of as one broad feature having two shoulders: the one with lower frequency, AS_1, is due to the in phase vibration of adjacent oxygen atoms, while the higher frequency one, AS_2, is due to 180° out of phase motion of the adjacent oxygen atoms [6].

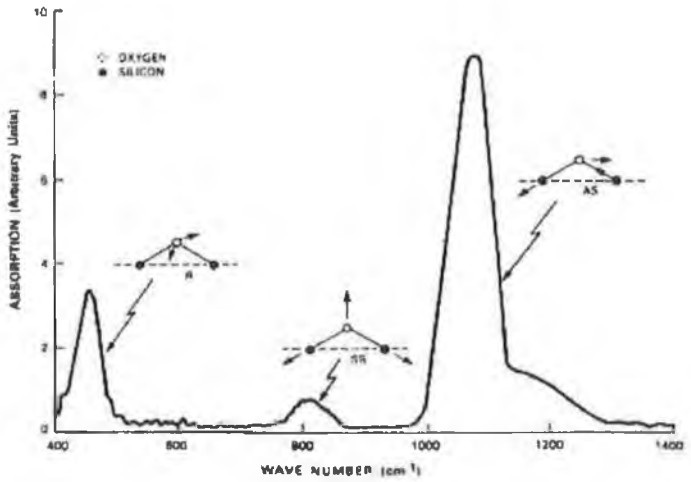

(a)

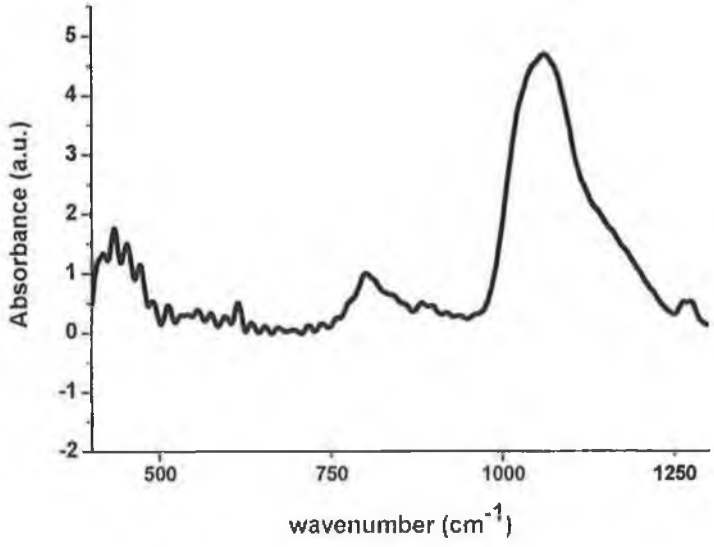

(b)

Figure 4.11: Infrared absorption spectrum; (a) taken from literature [6]; (b) measured in our laboratory for 180nm thick a-SiO_2 oxide film grown thermally on silicon. Both spectra show the spectral signatures associated with rocking, symmetrical stretching and asymmetrical stretching vibrational motions

While knowledge of the microscopic origin of the peaks is not always necessary for certain applications, generally it will provide an enhanced appreciation of the sample under investigation.

References

[1] B. C. Smith, Fundamentals of Fourier Transform Infrared Spectroscopy, CRC Press, 1996.

[2] Smith, Applied Infrared Spectroscopy, John Wiley and Sons, 1979

[3] Nicolet Instrument Corporation, User's Guide to Nexus FTIR spectrometer,2001.

[4] S.Coran, Corso di Analisi dei Farmaci III, Introduzione a FTIR e tecniche di campionamento.

[5] C.T.Kirk, "Quantitative analysis of the effect of disorder-induced mode coupling on infrared absorption silica", Physical review B, Vol.38, n.2.

[6] R.J. Bell "Introductory Fourier Transform Spectroscopy", Academic Press, 1972 (& references therein).

CHAPTER 5: SAMPLES ANALYSIS; RESULTS AND DISCUSSION

Due to the relevance of fluorocarbon plasma etching of SiO_2 and ultra-low dielectric constant films as an important step in integrated circuit manufacturing, it would be useful to optimize the plasma process. The optimization has been generally found to be challenging due to the complexity of fluorocarbon plasma etch mechanism, ion fluxes and energies, and processes of molecular dissociation. This requires a proper investigation of the composition of the films on the sample surface and the comprehension of the radical kinetics of the polymer films deposition due to etching [1, 2]. A mechanistic understanding of plasma-surface interactions in the etching process of silicon dioxide and other dielectrics by fluorocarbon plasmas is moreover critical to the development of predictive models for plasma process design [3] and this is the reason for which our project has been focused on the investigation of etched SiO_2 and ultra low-k material (ULK), and in particular on the possible changes in material composition due to etching. Etching processes which change the C and/or F concentrations can lead to unintended changes in the k value, and the ability to monitor changes in these concentrations using basic FTIR spectroscopy would be a useful off-line tool as mentioned earlier. This study was made on samples provided by Intel-Ireland.

5.1: SiO_2 films

5.1(a): Brief general overview of SiO_2

SiO_2 is formed by strong directional covalent bonds arranged in a well-defined local structure: four oxygen atoms are arrayed at the corners of a tetrahedron around a central silicon atom (Figure 5.1a). The bond angles for O-Si-O are 109 degrees; the Si-O distance is generally 1.61Å (0.161 nm). The bond distance is actually slightly smaller than the sum of the conventional covalent "radii" of the atoms: Si (0.110 nm) + O (0.066

nm) ≈ 0.18 nm. Thus in reality the atoms should be depicted as slightly penetrating each other (Figure 5.1b).

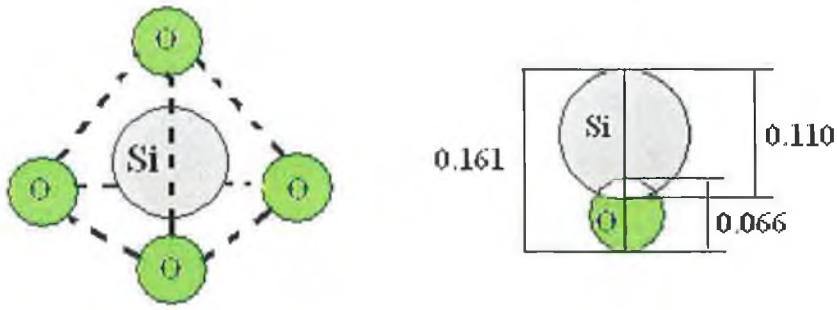

(a) (b)

Figure 5.1: (a) Schematic structure of the silicate tetrahedron; (b) interpenetrating electronic 'radii' of silicon and oxygen in SiO_4

The bond angle between Si-O-Si is nominally about 145 degrees, but can vary from 100 to 170 degrees with very little change in bond energy. Furthermore rotation about the axis is almost completely free (Figure 5.2). A convenient way of summarizing these observations is that the 'tetrahedra' formed by the SiO_4 groups must touch each other at their corners, but they can do so over a wide range of angles.

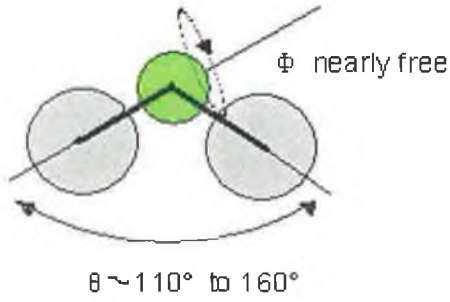

Figure 5.2: Schematic representation of Si-O-Si bond angles

This results in flexibility in the bridge bonds in SiO_2 so that, because they may have many different possible orientations, they can very easily form amorphous materials (i.e. materials with no long-range order). Essentially all deposited and thermally grown oxides in semiconductor processing are amorphous.

5.1(b): Analysis of the SiO_2 samples

The analyses on these samples were carried out to investigate the influence of C_4F_8 / Ar / O_2 plasma etching on the SiO_2 films: the aim being to determine the potential of FTIR as a technique to understand how the chemical composition of the SiO_2 films are altered in a commercial reactor as a function of changes in the feed gases and the exposure time to the etching plasma. A silicon oxide wafer received from Intel, was cut into several pieces and each of them processed with a different plasma treatment.

The preliminary plasma-assisted etching on the samples was carried out in a commercial RF reactor (Chapter 3, section 3.6) using a C_4F_8 / Ar / O_2 chemistry; subsequently we have used gas mixtures with either C_4F_8 / O_2 or C_4F_8 / Ar in order to understand the separate effect of the two gases on the surface chemistry. The different etching chemistries were carried out at several different exposure times: this helps to evaluate the etch rate on the oxide surface. The etching processes were carried out at RF powers inside the reactor between 700W and 1200W together with the experimental parameters listed in table 5.1.

Table 5.1: Plasma experiments carried out.

Plasma Composition	C_4F_8 Flow [sccm]	O_2 flow [sccm]	Ar Flow [sccm]	Pressure [mtorr]
C_4F_8/ Ar/ O_2	40	50	200	65
C_4F_8/ Ar	40		200	65
C_4F_8/ O_2	40	100		65

To get a comprehensive overview of the dynamics of the process, the analysis has been carried out by varying the exposure time for each of the three chemistries. Using this method it is possible to get an indication of the effect of the chemistry on the etch rate. The exposure times investigated in this experiment were 1, 2, 4 and 6 min. Figure 5.3 shows the spectroscopic ellipsometry measurements of the SiO_2 layer's thickness as a function of etch chemistries and times. The thicknesses of the samples have been

determined by ellipsometry measurements. Ellipsometry is very sensitive measurement technique which uses polarized light to characterize thin films and surfaces [4]. An incoming light beam of a known polarization state is incident on the sample and the ellipsometer measures the change in the reflected beam's polarization. In particular the ellipsometer used was a J.A.Woollam single wavelength ellipsometer, and the samples were tested at a 623.8 nm wavelength.

The C_4F_8 / Ar chemistry is seen to produce a linear etch rate* with time which is significantly faster than either of the other two chemistries containing oxygen; the latter, in turn, shows comparable removal rates. This indicates that the presence of oxygen in the plasma composition hinders the etch rate to a considerable extent.

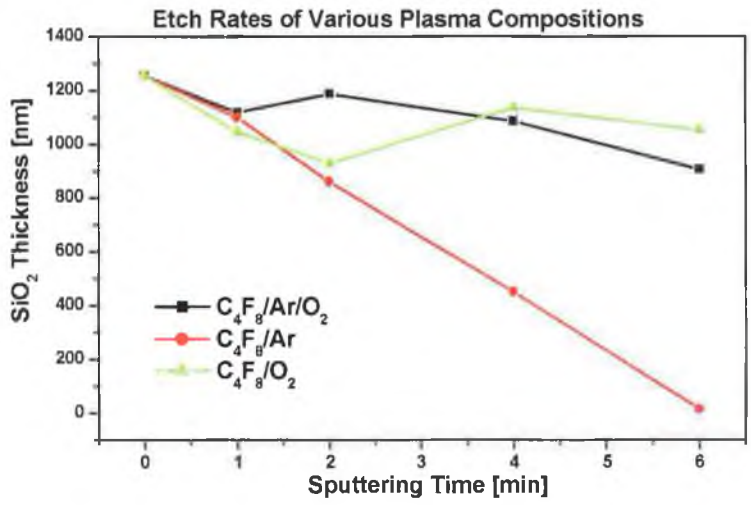

Figure 5.3: Thicknesses of the oxide layers measured by ellipsometry

This finds confirmation in the infra red analysis carried out, where the sample etched at six minutes of exposure time with fluorocarbon and argon shows very low absolute values of absorbance (figure 5.4a). The FTIR spectra of the sample etched in the C_4F_8 / Ar mixture show a reduction in the SiO_2 features as the etch time increases from 1 to 6 minutes (at which point the oxide layer thickness reduces to that of the native oxide in the

* The etch rate is defined as the slope of the best fit line describing the ratio vs. exposure time in the range in which this ratio is approximately linear.

background sample). The correlation of the thicknesses estimated from the FTIR data with the data from figure 5.3 is shown in figure 5.4(b) and is very good. Figure 5.4(c) shows the spectra for the sample etched in the C_4F_8 / O_2 mixture, and we observe here a very significant reduction in etch rate compared to figure 5.4(a), which was also seen for this gas mixture in the data in figure 5.3. Again the correlation of the thicknesses estimated from the FTIR data with the data from figure 5.3 is shown in figure 5.4(d). Data similar to figure 5.4(c) and 5.4(d) are also seen for the C_4F_8 / O_2 / Ar gas mixture.

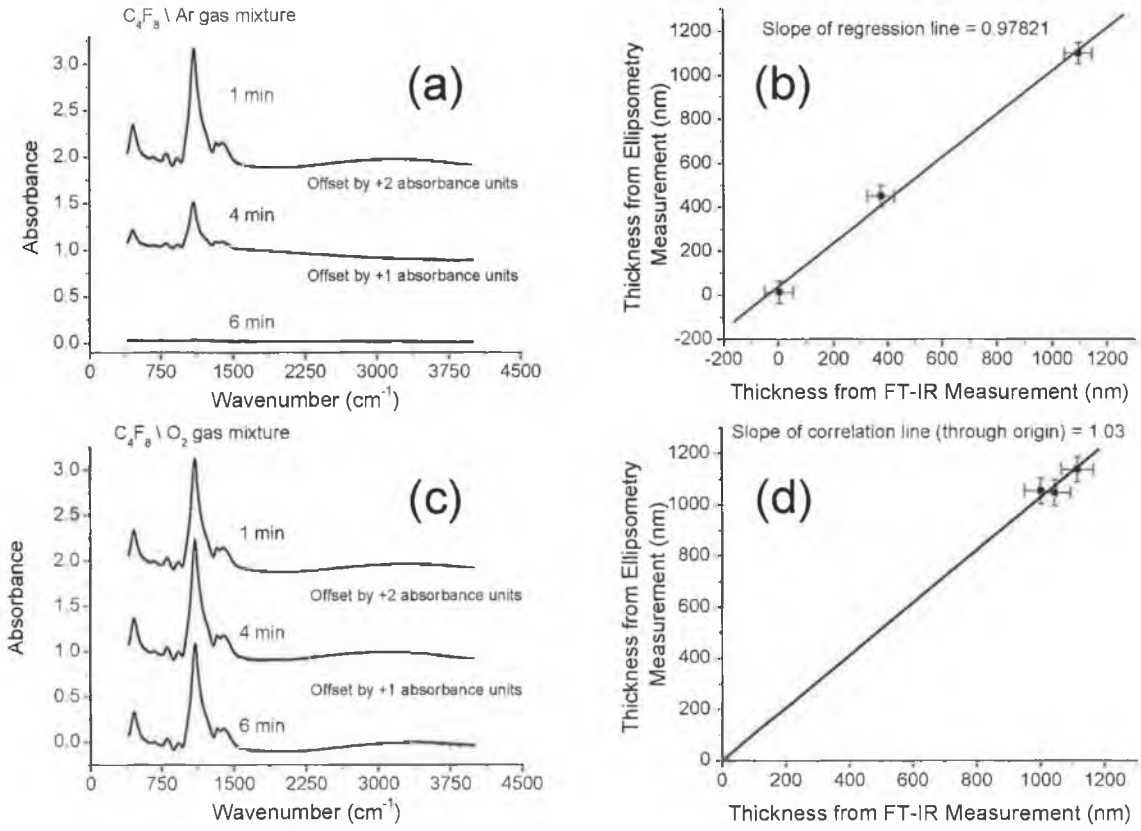

Figure 5.4: (a) FTIR spectra of SiO_2 layers after etching in C_4F_8 / Ar mixture, demonstrating the etching effect of this gas mixture. (b) Correlation of data in subfigure (a) with ellipsometer data in figure 5.3 above. (c) FTIR spectra of SiO_2 layers after etching in C_4F_8 / O_2 mixture, demonstrating the reduction in etch rate compared to subfigure (a). (d) Correlation of data in subfigure (c) with ellipsometer data in figure 5.3 above. The error bar on the thickness measurements is ± 4nm for both techniques

The thickness values were calculated from the FTIR data using a relative measurement in which the area under the absorbance curve is the quantity directly related to the thickness of the sample. Assuming that the integrated absorption between ~ 900cm^{-1} and 1900 cm^{-1} of the sample etched for 1 minute matches the thickness of the ellipsometer data, the integrated absorption in the same range for the other samples were ratioed in proportion in order to get the equivalent FTIR thickness for other samples.

Thus the FTIR data agrees well with the data from ellipsometry measurements concerning bulk etching rates and is also in agreement with the results XPS (X-ray Photoelectron Spectroscopy) and SIMS (Secondary Ion Mass Spectroscopy) analyses [1].

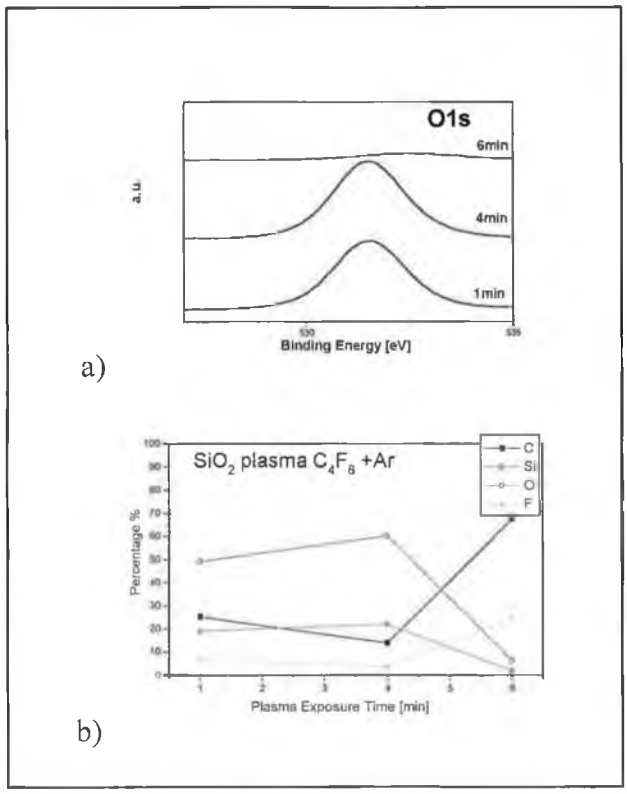

Figure 5.5: XPS profile of O1s peak after C_4F_8/Ar plasma etching (a); XPS depth profile showing the composition of the surface after different durations of C_4F_8/Ar plasma chemistry etching (b).

In figure 5.5 (a) is possible to see how the XPS profile of the O1s peak in the sample etched with C_4F_8 / Ar plasma chemistry gradually decreases with sputtering time, and this

compares well with the results shown in figure 5.4(a), (b).As well, in figure 5.5 (b) the surface elemental composition (as determined by XPS) of the C_4F_8 / Ar etched samples shows that after 6 min. sputtering time the concentrations of oxygen and silicon decrease due to removal of the SiO_2 layer and the concentrations of carbon and fluorine increase due to the formation of the polymeric film.

The film thickness is strongly dependent on the presence of an oxygen source in the system, either via the plasma gas mix or from the SiO_2 substrate. When oxygen is present this film remains quite thin, and will not, of itself, inhibit etching, as observed for the C_4F_8 / Ar plasma. However, the presence of oxygen in the plasma reduces the etch rate significantly as active sites for fluorine adsorption are blocked [1, 5].

Therefore, the conclusion is that there is a considerable reduction of the dioxide layer on the sample surface following the etching chemistry with C_4F_8 / Ar only. In combination with XPS and SIMS analyses [1, 6] this has been shown to be due to the presence of a polymeric-type hydro-fluorocarbon film formation. The presence of this film is a crucial factor in the competition between formation of Si-C bonds, formation of some bonds of the type C-F-H in the polymer network and the etching process. In figure 5.6 a scheme of the adsorption mechanism of CF radicals on the SiO_2 surface and the role of Ar ion bombardment is shown. CF radicals are adsorbed as shown in figure 5.6 and the C-F bond is stretched and eventually broken, with subsequent bond formation between these adsorbed species and atoms on the surface: the kinetic energy provided by the Argon ion bombardment disrupts the bonding in the near surface region increasing the reactivity with the gaseous plasma species. However, when oxygen is present in the plasma, the etch rate is significantly reduced because active sites for fluorine adsorption and polymer film growth are largely blocked. This prevents the fluorine etch mechanism and also inhibits the polymeric film growth [1].

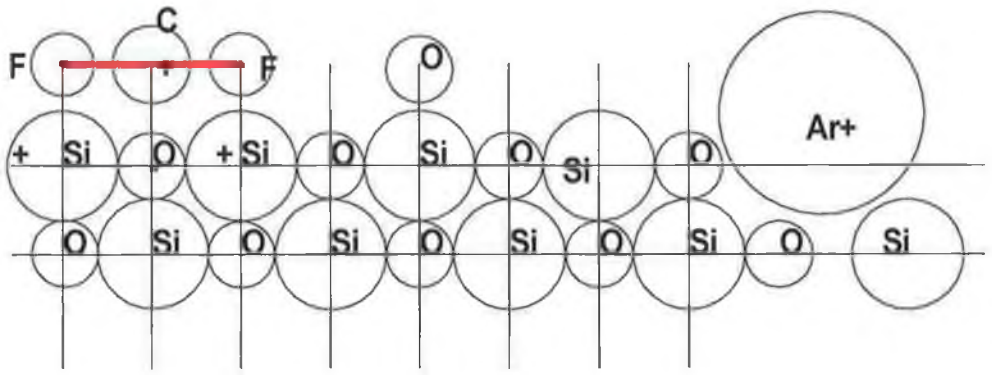

Figure 5.6: Schematic of adsorption of CF radicals on SiO_2 surface and Ar+ ion bombardment [1]

The next point of investigation concerns the effects of the etching in various gas atmospheres on the chemical composition of the thin film (which may have important consequences for the dielectric constant of the films). In the infrared spectra the characteristic peaks of amorphous SiO_2 (figures. 5.7, 5.8, 5.9 and 5.10) already discussed in Ch.4 (figure 4.9) can be seen, with the addition of the C-O bending vibration peak at around 667 cm^{-1} (figure 5.8) and of the C-F stretching vibrations group, whose frequencies have been found to range in the interval 1400-1000 cm^{-1} (figure 5.10) [7]. Though, it is not possible to establish to which specific group (CF, CF_2, CF_3) such vibrations, related to CF_x -like structures, belong to. This impossibility is due to the strong coupling between these molecular vibrations, leading to a probable superimpositions of the related peaks. Therefore, XPS is useful in such a situation, being able to separate the functional group. The peak at around 806cm^{-1} in figure 5.8 may be associated either with the Si-CH_3 bending vibration that occurs at 802 cm^{-1} or with the Si-O symmetrical bending vibration at 810 cm^{-1} [8] (the spectral resolution of the FTIR system is 4cm^{-1}). It is most likely due to a combination of both these peaks. As can be seen from all these figures, etching in a C_4F_8/Ar mixture removes almost all the oxide from the substrate after 6 minutes exposure as it is the case in figure 5.4 above: it is also evident in the decreased absorbance in the main two peaks associated with Si-O bonds (figure 5.7, figure 5.9).

In particular, some of the vibrations in the mid-IR region are sensitive to the presence of F in the material. Consequently we have looked for evidence of changes in these peaks in our material, particularly after etching in the C_4F_8/Ar mix, where the deposition of the C-F-H polymer film may lead to introduction of F into the oxide layer. The peak at ~ 925 cm^{-1} in figure 5.8 may be associated either to the Si-F stretching mode [8, 9] or the Si-H bending vibration, both of them occurring in the region between 930 cm^{-1} and 940 cm^{-1} [10]. The asymmetric stretching vibration peak at around 1100cm^{-1} has been reported to show a frequency shift towards higher wavenumbers with an increase of fluorine content [8]. However no significant changes in intensity of the 925 cm^{-1} peak or shifting of the 1100 cm^{-1} peak is observed in our spectra after etching, beyond changes in intensity due to removal of material via etching. All the features seen in the FTIR spectra disappear with increased etching time in the C_4F_8 / Ar mix, and appear to be much less sensitive to etching in mixtures containing O_2, and thus we believe that they are associated with the bulk region of the SiO_2 layer and are not associated with the polymer layer deposited during etching or species introduced into the oxide during etching.

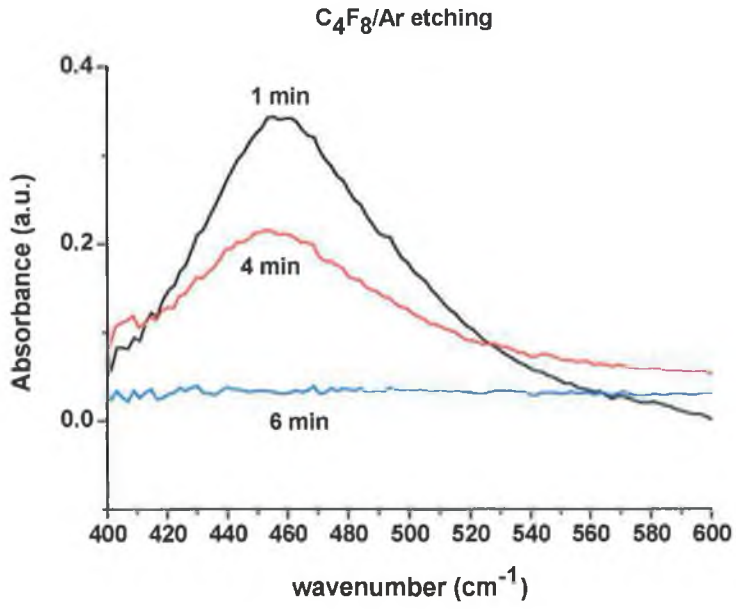

Figure 5.7: Si-O rocking vibration

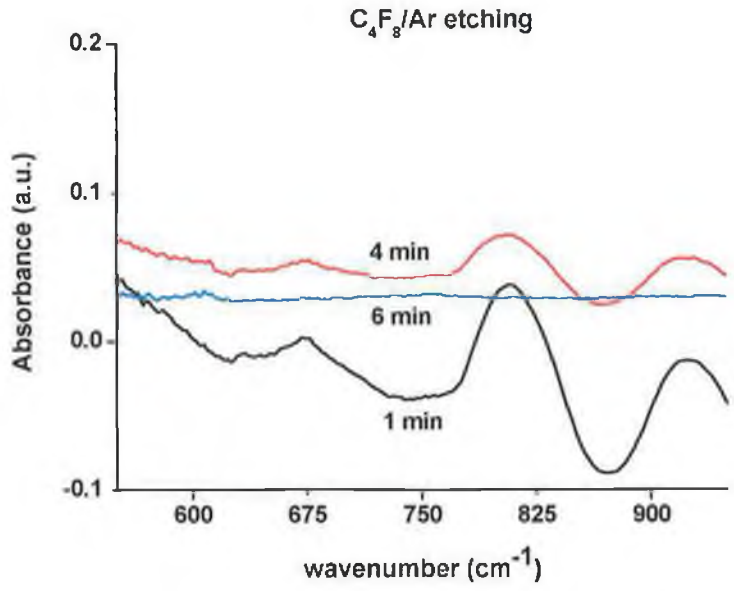

Figure 5.8: C-O , Si-O bending vibrations and Si-F bond

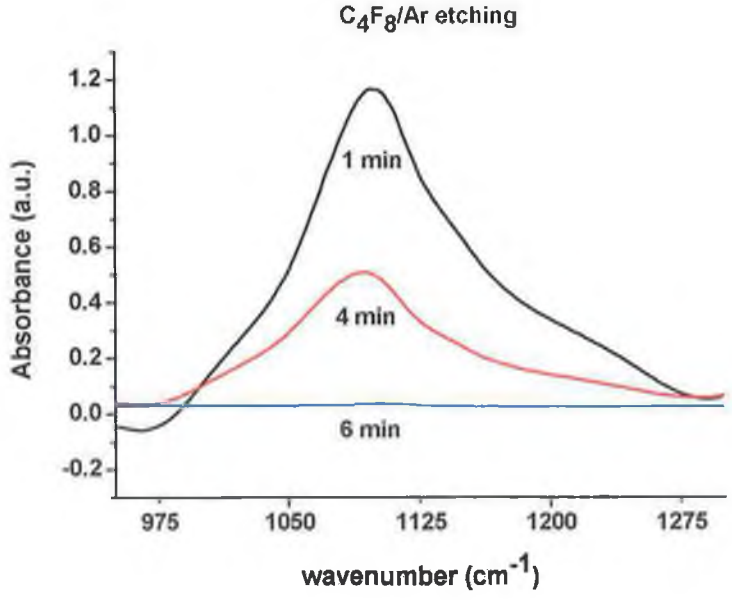

Figure 5.9: Si-O asymmetric stretching vibration

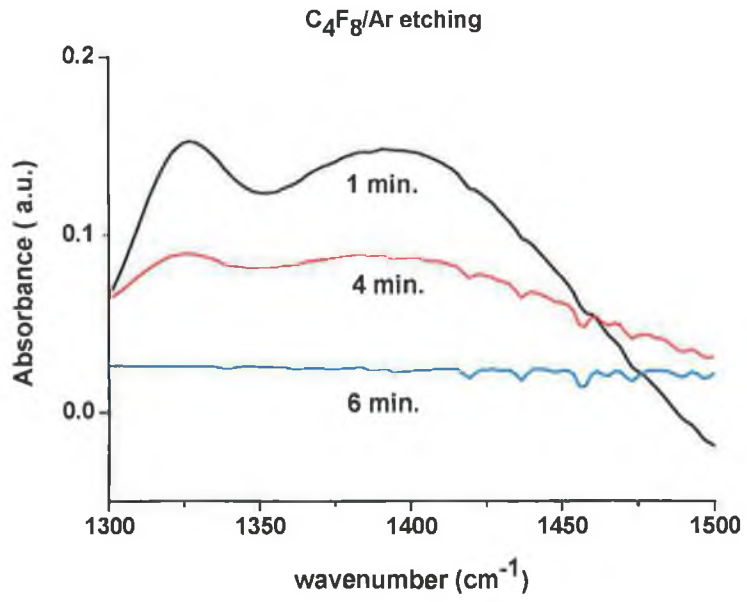

Figure 5.10: Si-CH3 stretching vibration and C-F stretching vibrations band

However there is no evidence of any changes in the peak shapes during etching in any of the samples indicating that any changes in the chemical composition of the samples and any dielectric poisoning effects due to either F or C are below our detection limit. We may roughly estimate our detection limits in terms of concentrations of species (per cm^2) in the beam path by using the FTIR and ellipsometer data shown previously in figure 5.4(b). We see no FTIR signal for thin layers, even though the ellipsometer data gives a finite value for the layer thickness of 13 nm. Thus we make a lower estimate of the detection limit of molecular species of this system by calculating the number of SiO_2 molecules per cm^2 in a 13nm SiO_2 thick layer. Using the known density of SiO_2 (~2.2 grams/cm^3) [11] we estimate that our detection limit for our system is ~10^{16} molecules/cm^2. Obviously this estimate is rather crude but nevertheless gives an order of magnitude feel for the detection limit. If we are interested in estimating the lower concentration levels of detectable impurity species in a thicker dielectric layer, ~1μm, we can also use the minimum detectable number of species ~ 10^{16} molecules/cm^2 to give a detectable concentration of ~ 10^{20} molecules/cm^3. In the case of ATR the detection limit is reported to be 10^{14}

molecules/cm^2 [12], which is ~ 2 orders of magnitude more sensitive than the standard FTIR configuration, as mentioned earlier.

5.2: Ultra- Low- dielectric constant (ULK) samples

This series of samples has as main features a low density and low dielectric constant (2.4-2.5). As already stated in the introduction, the importance of RC delay reduction in integrated circuits leads to a need for replacing the SiO_2 ($K \approx 4$) of the intermetal dielectric with a low dielectric constant material.

In figure 5.11 a) and b) the microscopic structure of the ULK layer and the section of a ULK sample are shown respectively, and in figure 5.12 the film composition as obtained from SIMS (secondary ion mass spectroscopy) analysis is shown [13]. The data are shown as received from the sample fabricating company ASM. Note that the fluorine content curve lies behind the nitrogen curve and is therefore not visible in the graph. The thicknesses of the ULK layers before etching treatments are ~ 100 nm.

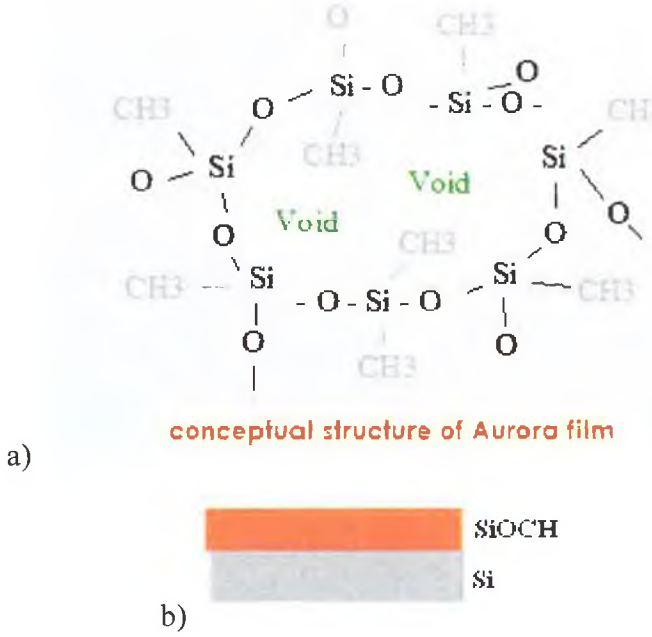

Figure 5.11: ULK material structure, (a) internal structure and (b) constitutive layers of the sample studied [13]

In order to exploit techniques compatible with the already existing silicon process technology, thin film layers are generally grown by Chemical Vapour Deposition (CVD) on a Si substrate. A certain percentage of porosity is introduced in the material in order to have a further reduction of the dielectric constant [14]. Such amorphous materials are from the group comprised of Si, C, O, H and are known by different names, including SiOCH, carbon-doped oxides (CDO), organosilicate glasses (OSG), silicon-oxicarbides [15].

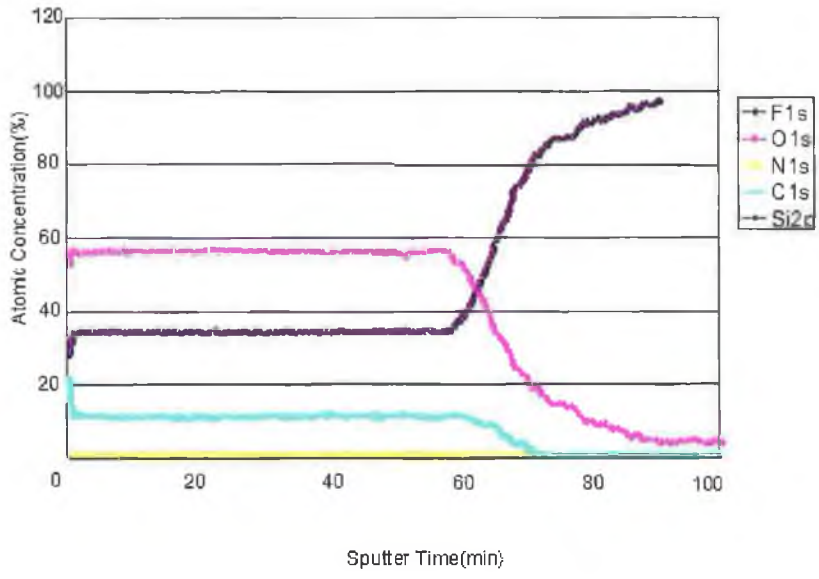

Si : 33 %, C : 11 %, O :56 %

Figure 5.12: Depth profile of the ULK samples as received [13]

5.2(a): Statistical Design of Experiment (DOE)

The aim of the study of this series of samples is to determine how the chemical composition of the ULK layer is altered as a result of changes in the chemical composition of feed gases and applied power in a commercial reactor. To investigate such effects, which involve a large parameter space with unknown cross-interdependencies, it is necessary to employ a reliable systematic method that minimizes

the number of factors involved. Design of experiments (DOE) is a technique used to minimise the number of experiments to be carried out when a large number of variables (design factors) with a large number of levels are present without compromising on data gained. It consists of a group of experiments performed in order to study the relation between the process variables and the process response parameters [16]. A screening experiment is necessary to determine the parameters to be involved in the DOE and to eliminate useless ones. The screening experiment is done by statistical methods at the beginning based on which variables are likely to control the process under examination.
The space of variables involved in the design of experiment has been determined using the Tagouchi method [17]. This method suits the case of plasma etching, where the process is a function of the different factors inside the reaction chamber.
There necessarily are, as well, a certain number of casual factors which was not accounted for in the DOE: such as condition of the chamber wall, possible residual deposition on the chamber wall, temperatures of the chamber wall, time elapse between sample processing and measurement, environmental situation. It was not possible to account for those factors, because of the impossibility of measuring or controlling them.
The DOE analysis was performed for us by collaborators from Intel Ireland, who recommended the best range of reactor parameters to use for our experiments on ULK material.

The result of design of experiment has been a set of 18 experiments involving 6 variables, listed in table 5.2, and the samples were named according to a sequence starting with P0 and ending at P18. The second column in the table contains the patterns of the experiment control variables listed in columns three to five. Each control variable has two possible values that could be used, either maximum or minimum. The pattern is composed of five signs in a series of either (+/-). The (+) and (-) signs indicate the variable's level, maximum or minimum, respectively.

Table 5.2: DOE design for carrying out the experiments on ULK samples.

	Pattern	Upper Power (W)	Lower Power (W)	O_2 flow (sccm)	C_4F_8 flow (sccm)	Pressure (mtorr)	Ar (sccm)
P0							
P1	-++-+	1200	600	45	15	45	300
P2	--+--	1200	200	45	15	15	300
P3	+++++	600	600	45	45	45	300
P4	-+-++	1200	600	15	45	45	300
P5	-+---	1200	600	15	15	15	300
P6	++-+	600	600	15	45	15	300
P7	+----	600	200	15	15	15	300
P8	-+++-	1200	600	45	45	15	300
P9	---+-	1200	200	15	45	15	300
P10	----+	1200	200	15	15	45	300
P11	11111	1200	200	15	15	15	300
P12	--+++	1200	200	45	45	45	300
P13	+-++-	600	200	45	45	15	300
P14	+--++	600	200	15	45	45	300
P15	+-+-+	600	200	45	15	45	300
P16	++--+	600	600	15	15	45	300
P17	+++--	600	600	45	15	15	300
P18	11112	1200	200	15	15	45	300

5.2(b): Analysis of ULK samples

From the infrared analysis of this series of samples no systematic correlation between etching process and FTIR characteristics of any of the spectra was found. The FTIR spectra in figures 5.13, 5.14 and 5.15 look like typical spectra of SiO_2-like complexes and only some of them show occasional peak that might be due to Si-F bonds, but with no systematic appearance which correlates to the parameters in the reaction chamber. For sample P16, figure 5.16 shows a peak at 940 cm^{-1}, that can also be clearly seen in the broader spectrum in figure 5.15. This peak has been associated to molecular vibration of the Si-F bond, which in the literature is reported as centered around 940 cm^{-1} [8, 9,18].

A common feature of all the absorbance spectra is, moreover, the band occurring in the range between 700 cm^{-1} and 900 cm^{-1}: this is probably due a convolution of vibrational mode of Si-C bond, Si-H bond and Si-O bending mode. Such peaks are reported in literature as occurring respectively centered at 800 cm^{-1}, 798 cm^{-1}, 840 cm^{-1} [19, 13].

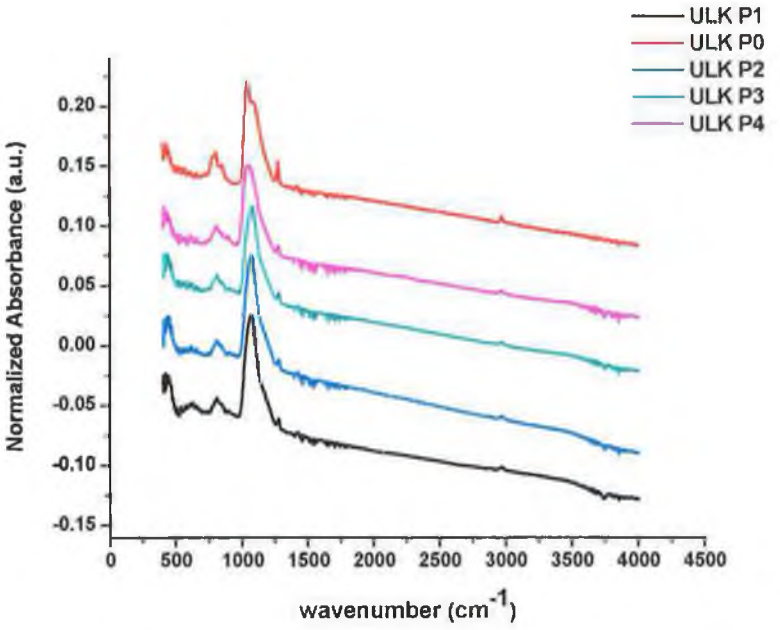

Figure 5.13: Absorbance spectra of the ULK samples P0 to P4

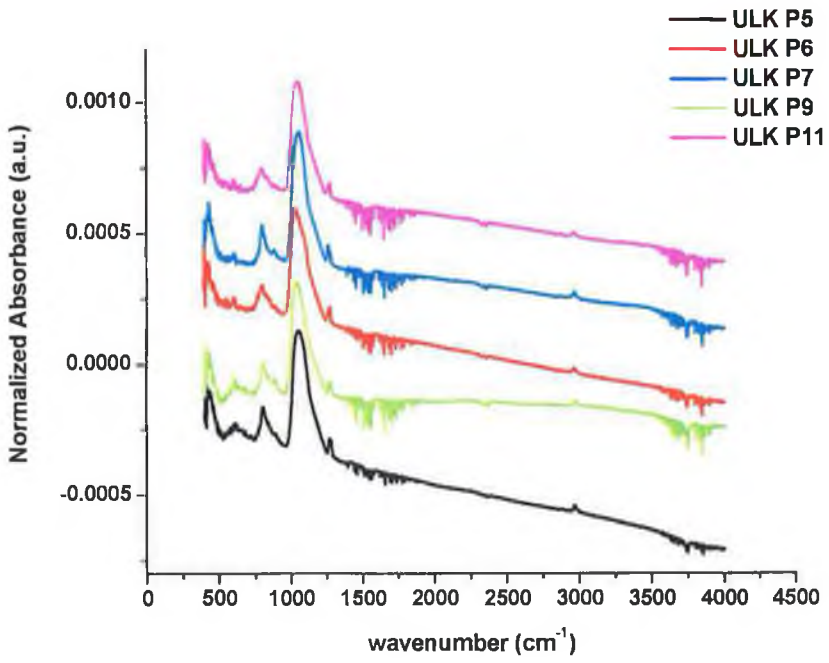

Figure 5.14: Absorbance spectra of the ULK samples P5 to P7, P9 and P11

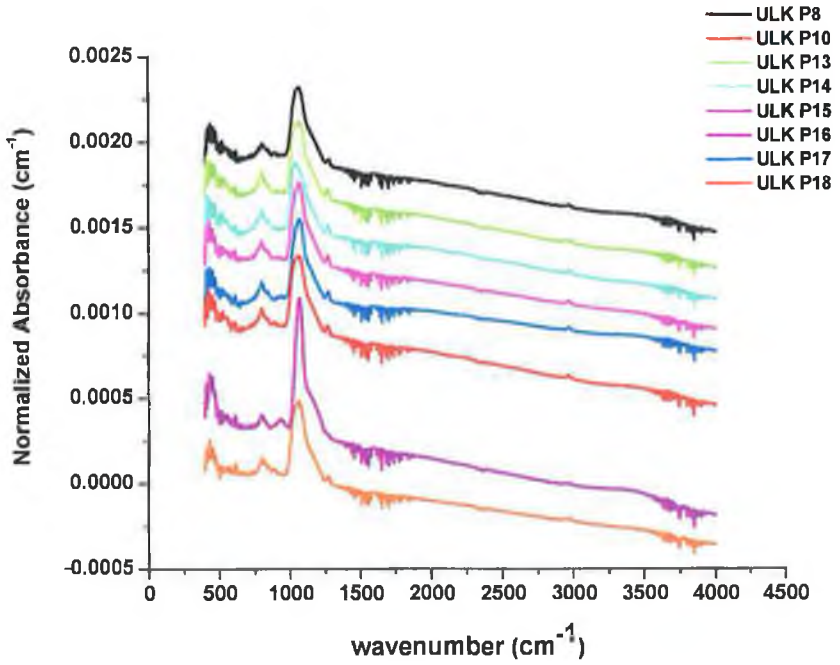

Figure 5.15: Absorbance spectra of the ULK samples P8, P10 and P13 to P18

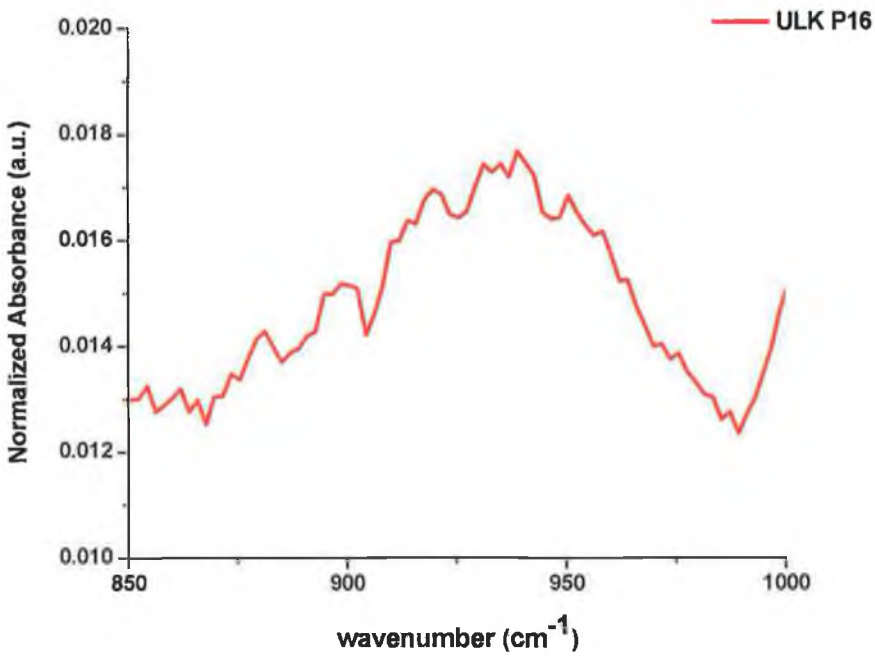

Figure 5.16: The peak corresponding to Si-F bond in sample P16

In conclusion, in the case of the ULK samples, we again see no systematic variations in the FTIR spectra for different plasma processing conditions which can be reliably indexed to changes in C and F concentrations and correlated to the process parameters. XPS and SIMS, whose main significant results are at stretch reported, do however indicate a reduction in the C concentration close to the surface of the ULK layer except in the samples etched according to process 4 and 9 of table 5.2 [20]. Thus, we conclude that the basic FTIR spectroscopy set-up we have used is not sensitive enough to detect these changes.

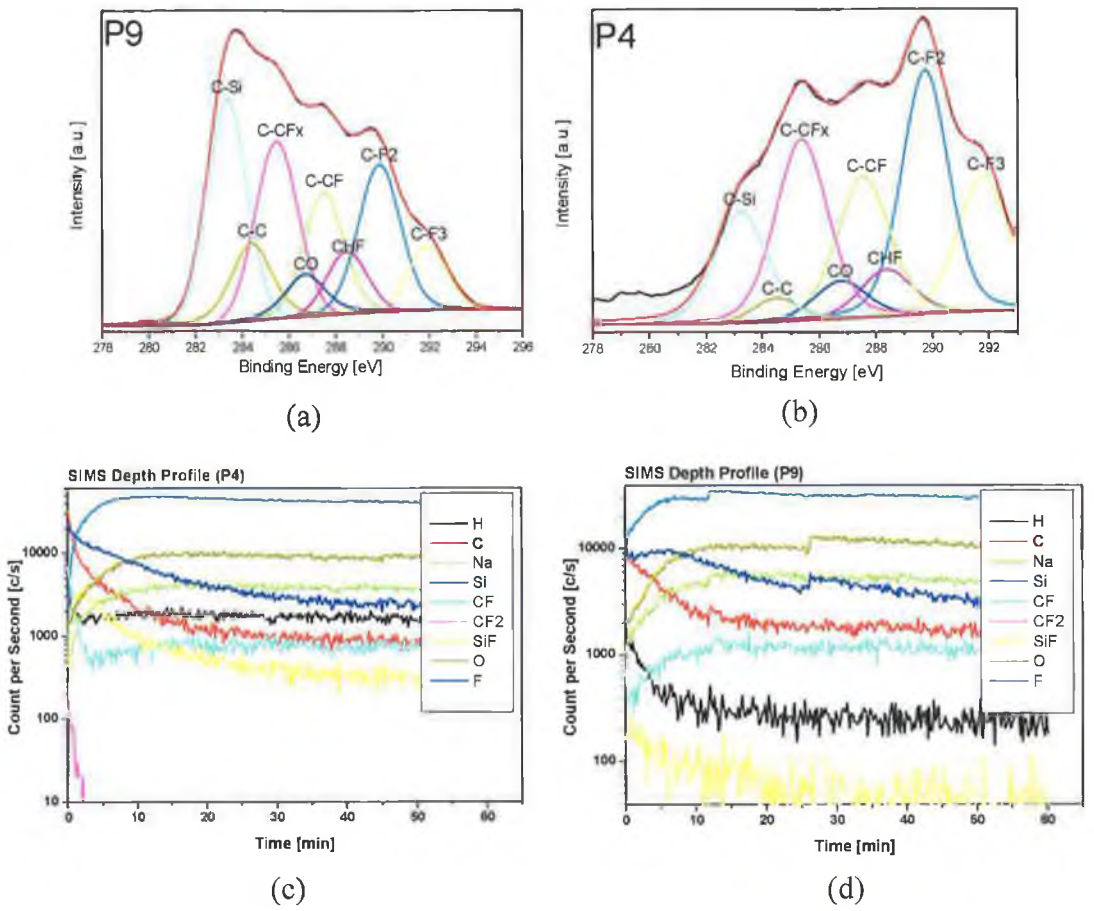

Figure 5.17: C1s peak from XPS analysis on the surface after plasma etch according to (a) process 4 and (b) 9 from table 5.2, showing peak deconvolution and the various bonds between the fluorine and the carbon; SIMS depth profiles of the sample etched according to (c) process 4 and (d) of the sample etched according process 9. Profile of C1s peak after process 4 is mirror image of that after process 9. The former has its maximum at higher binding energies. This is due to the fact that maximum value of lower power produces ions with higher kinetic energy, which form stronger bonds characterized by higher binding energy. By looking at the first five minutes in the SIMS profiles it is possible to see there is abundance of carbon and fluorine species on the surface, in agreement with the XPS data.

Process 4 and process 9, in fact, yield the thickest C-F-H polymer films based on XPS and SIMS data shown above. This indicates that upper power significantly promotes

fluorocarbon bonding. The carbon peak profile in figure 5.17 (a), (b) is evidence of polymeric-type hydrofluorocarbon film formation due to competition between formation of Si-C bonds, formation of some bonds of the type C-F-H polymer network and etching process itself.

The above mentioned processes also have minimum oxygen flow which could oxidise CF radicals and prevent polymer film formation. The process P4 and P9 are both characterized by maximum C_4F_8 flow, which favours the polymer film formation. But while in the case of process 4 the lower power and the pressure are maximum, in the case of process 9 lower power and pressure have their minimum value. The ion energy is proportional to the lower power and inversely proportional to the current (plasma density, pressure). The fact that in the case of process 9 the etching rate is higher than in the case of process 4 could be explained by being due to the higher ion energy (as a consequence of lower ion current). Profile of C1s peak after process 4 is a mirror image of that after process 9. The former has its maximum at higher binding energies [21, 5].

References

[1] V.Krastev, I.Reid, C.Galassi, G.Huges and E.McGlynn, 'Influence of $C_4F_8/Ar/O_2$ plasma etching on SiO_2 surface chemistry ', Journal of Materials Science: materials in electronincs, 16(2005), p.541-547.

[2] X.Li, L.Ling, X.Hua, M.Fukasawa and G.S.Oehrlein, 'Effects of Ar and additives on SiO_2 etching in C_4F_8-based plasmas', J.Vac.Sci.Technol.A 21(1), Jan/Feb 2003.

[3] D.C.Gray and H.H. Savin, 'Quantification of surface film formation effects in fluorocarbon plasma etching of polysilicon', J.Vac.Sci.Technol.A 9(3), May/Jun 1991.

[4] http://www.jawoollam.com/tutorial_1.html, "Woollam Spectroscopic Ellipsometers and Thin Film Characterization", 29/08/05.

[5] Data courtesy of Ms.Ian Reid and Doctor Vesselin Krastev.

[6] Private communications from Ian Reid.

[7] J.Meichsner, K.Li, " In situ characterization of thin-film formation in molecular low-temperature plasmas", Appl.Phys. A 72, 565-571 (2001).

[8] Yoon-Hae Kim, Moo Sung Hwang, hyeong Joon Kim, Jin Yong kim, Young Lee, "Infrared spectroscopy study of low-dielectric-constant fluorine-incorporated and carbon-incorporated silicon oxide films", Journal of Applied Physics, vol.90, num.7, 2001.

[9] Kim, Kang, "FTIR study of fluorinated silicon oxide film", J. Phys.D:Appl.Phys.30 1720-1724.

[10] Colthup, Daly, Wiberley "Infrared and Raman Spectroscopy" (ag.31-32, 359).

[11] www.memset.org/material/silicondioxide, 06/09/2005.

[12] Akihito Shinozaki, Kenta Arima, Mizuko morita, Isao Kojima, Yasushi Azuma, " FTIR-ATR Evaluation of Organic Contaminants Cleaning Methods for SiO_2 Surfaces", Analytical Sciences, Nov.2003, Vol.19.

[13] Information about the samples prepared by ASM Japan Process Group, ULK Project team.

[14] D.Shamiryan, M.R. Baklanov, S.Vanhaelemeersch, K.Maex, "Comparative study of SiOCH low-k films with varied porosity interacting with etching and cleaning plasma", J.Vac. Sci. Technol. B 20(5), Sept/Oct 2002.

[15] A. Grill, D. A. Neumayer, "Structure of low dielectric constant to extreme low dielectric constant SiOCH films: Fourier transform infrared spectroscopy characterization", Journal of applied physics, Vol.94, n.10.

[16] R.H.Myers," Response Surface Methodology: Process and Product Optimization using Designed Experiments", John Wiley and Sons, 1995.

[17] http://www.ee.iitb.ac.in/~apte/CV_PRA_TAGOUCHI_INTRO.htm, 02/11/2004.

[18] Sang M.Han, Eray S.Aydil, "Structure and chemical composition of fluorinated SiO_2 films deposited using SiF_4/O_2 plasmas", J.Vac.Sci.Technol. A15(6), Nov/Dec 1997.

[19] Shi-Jin Ding, Li Chen, Xin-Gong Wan, Peng-Fei Wang, Jian-Yun Zhang, David wei Zhang,m Ji-Tao Wang, "Structure characterization of carbon and fluorine-doped silicon oxide films with low dielectric constant", Materials Chemistry and Physics, 71 (2001).

[20] V.Krastev, I.Reid, G.Hughes, L.Oksuz, B.Ellingboe, A.Isliakin, V. Milosavljevic " Investigation of space variables in C_4F_8 /Ar/O_2", in press, J. Mat. Sci.

[21] I.Reid, V.Krastev, G.Hughes, "Suppression of carbon depletion from carbon-doped low-k dielectric layers during fluorocarbon based plasma etching", in press, J.Mat.Sci.

CHAPTER 6: CONCLUSIONS AND RECOMMENDATIONS

Based on the results discussed in chapter 5, we can observe that the FTIR analysis is complementary to and agrees with the other techniques used, such as SIMS and spectroscopic ellipsometry, in the investigation of the plasma etching behaviour of the SiO_2 samples. The different etching rates in different gas mixtures have been associated with the blocking of fluorine adsorption sites by oxygen in the gas mixture which hinders the etch process.

We have further investigated the variation of peak position and shape during the etching process in an attempt to measure changes in the chemical composition of the oxide films and in particular changes in the C and F concentrations. However, no evidence is seen for either peak shifts or changes in peak shape associated with these contaminants, beyond the reduction in peak areas during the etching process.

For the second series of low-k dielectric samples examined (ULK), we have used a variety of etching procedures based on a design of experiment analysis to indicate the process parameters. The FTIR analysis doesn't show any systematic correlation between the absorbance spectra features and the plasma treatments performed: absorption peaks which may be related to the presence of F or C occasionally appear in various samples but show no systematic correlation to the process parameters. The overall features of the spectra resemble the typical silicon dioxide spectra.

Based on our data we may conclude that the basic FTIR system used is not sensitive enough to detect changes in the C or F concentrations in such dielectric materials, and hence cannot be used as a simple off-line tool for such analyses. In turn this probably indicates that the changes in such concentrations (in the range of process parameters we have examined), which have been noted in SIMS and XPS measurements, are quite localised at the surface (~20 nm), and consequently not easily detectible by our

apparatus, due to the fact that infrared spectroscopy gives a response through the whole thickness of the surface layer rather than in the very near surface region.

While these results are somewhat disappointing, they do allow us to comment definitively on the potential of the apparatus for such analysis, and to make some reasonably definite recommendation for future, optically-based, studies of such systems.

The key aspect required for optical studies of such species is a large increase in surface sensitivity. Hence techniques such as attenuated total reflection (ATR), where a surface localised evanescent wave probes the near boundary region are much more likely to yield positive detection of dielectric poisoning. The evanescent field combined with the longer interaction path length associated with multiple reflections in the guiding layer provide much higher surface sensitivity [1, 2].

This technique may be implemented with our FTIR spectrometer with an ATR add-on which may be purchased. However it is worth noting that the ATR requirement that the sample be in very close physical proximity to the ATR crystal (effectively butted against it) may have some negative repercussions if on-line analysis techniques are required in the future. In addition the sample must be a fixed (and rather small) dimension, which would make it difficult to measure data from a broad area of a semiconductor wafer.

Further optical studies based on the ATR technique, in combination with SIMS and XPS, in order to quantify the data appears to be the most promising route forward for quantitative optical characterisation of dielectric poisoning effects.

References

[1] A. Lee Smith, "Applied infrared spectroscopy: fundamentals, techniques and analytical problem-solving", John Wiley and Sons, 1979.

[2] Brian C. Smith, " Fundamentals of Fourier transform infrared spectroscopy", CRC Press, 1996.